

Tsunami inundation modelling for Lyttelton and Akaroa Harbours

1:500-year event from South America

Prepared for Christchurch City Council

May 2018

Prepared by:
Cyprien Bosserelle
Emily Lane



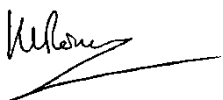
For any information regarding this report please contact:

Cyprien Bosserelle
Hydrodynamics Modeller
Hydrodynamics
89873483+64
cyprien.bosserelle@niwa.co.nz

National Institute of Water & Atmospheric Research Ltd
PO Box 8602
Riccarton
Christchurch 8011

Phone +64 3 348 8987

NIWA CLIENT REPORT No: 2018111CH
Report date: May 2018
NIWA Project: CCC18506

Quality Assurance Statement		
	Reviewed by:	Shaun Williams
	Formatting checked by:	Fenella Falconer
	Approved for release by:	Helen Rouse

© All rights reserved. This publication may not be reproduced or copied in any form without the permission of the copyright owner(s). Such permission is only to be given in accordance with the terms of the client's contract with NIWA. This copyright extends to all forms of copying and any storage of material in any kind of information retrieval system.

Whilst NIWA has used all reasonable endeavours to ensure that the information contained in this document is accurate, NIWA does not give any express or implied warranty as to the completeness of the information contained herein, or that it will be suitable for any purpose(s) other than those specifically contemplated during the Project or agreed by NIWA and the Client.

Contents

Executive summary	7
1 Introduction	8
1.1 Use of this report	8
1.2 Caveat	8
2 Methods.....	9
2.1 Models	9
2.2 Tsunami source	9
2.3 Trans-Pacific Tsunami Propagation.....	11
2.4 Local bathymetry/topography	12
2.5 Erosion evaluation	15
2.6 Validation	15
3 Results	17
3.1 Lyttelton Harbour	17
3.2 Akaroa Harbour.....	31
4 Discussion and Conclusion.....	44
5 References.....	45
6 Glossary of abbreviations and terms	47

Tables

Table 2-1:	Critical shear stress by particle-size classification for determining approximate condition for sediment.	15
------------	---	----

Figures

Figure 2-1:	Maximum wave height in Pegasus Bay resulting from a 20m slip earthquake applied at each fault unit in the SIFT database for South America.	10
Figure 2-2:	Fault segments involved in the Mw 9.28 earthquake scenario for 1:500-year tsunami inundation (highlighted in red).	10
Figure 2-3:	Maximum water level for the 1:500-year tsunami event trans-Pacific propagation.	11
Figure 2-4:	Nested grid extents used in ComMIT to propagate the tsunami waves to the Basilsik boundaries.	11

Figure 2-5:	Water levels at the entrance of Lyttelton and Akaroa harbours as simulated using ComMIT.	12
Figure 2-6:	Bathymetry and topography data collated to produce to produce the Lyttelton model grid.	13
Figure 2-7:	Lyttelton Harbour bathymetry grid as used in the Basilisk model.	13
Figure 2-8:	Akaroa Harbour bathymetry grid as used in the Basilisk model.	14
Figure 2-9:	Model validation for the Valdivia tsunami of 1960.	16
Figure 3-1:	Maximum inundation depth (i.e., height above ground) for 1:500-year return period event current sea level - Head of the Bay.	18
Figure 3-2:	Maximum inundation depth (i.e., height above ground) for 1:500-year return period event current sea level – Lyttelton and Diamond Harbour.	18
Figure 3-3:	Tsunami water level at the Port entrance for the three sea level scenarios.	19
Figure 3-4:	Tsunami water level at Teddington for the three sea level scenarios.	19
Figure 3-5:	Tsunami water level at the head of Purau Bay for the three sea level scenarios.	20
Figure 3-6:	Maximum inundation depth (i.e., height above ground) for 1:500-year return period event - 2065 sea level scenario – 0.41 m sea level rise - Head of the Bay.	20
Figure 3-7:	Maximum inundation depth (i.e., height above ground) for 1:500-year return period event - 2065 sea level scenario – 0.41 m sea level rise - Lyttelton and Diamond Harbour.	21
Figure 3-8:	Maximum inundation depth (i.e., height above ground) for 1:500-year return period event - 2120 sea level scenario – 1.06 m sea level rise - Head of the Bay.	21
Figure 3-9:	Maximum inundation depth (i.e., height above ground) for 1:500-year return period event - 2120 sea level scenario – 1.06 m sea level rise - Lyttelton and Diamond Harbour.	22
Figure 3-10:	Maximum flow velocity for 1:500-year return period event current sea level - Head of the Bay.	23
Figure 3-11:	Maximum flow velocity for 1:500-year return period event current sea level - Lyttelton and Diamond Harbour.	23
Figure 3-12:	Flow velocity at the port entrance for the three sea level scenarios.	24
Figure 3-13:	Flow velocity at Head of the Bay for the three sea level scenarios.	24
Figure 3-14:	Flow velocity at the head of Purau Bay for the three sea level scenarios.	25
Figure 3-15:	Maximum flow velocity for 1:500-year return period event 2065 sea level scenario – 0.41 m sea level rise - Head of the Bay.	25
Figure 3-16:	Maximum flow velocity for 1:500-year return period event 2065 sea level scenario – 0.41 m sea level rise - Lyttelton and Diamond Harbour.	26
Figure 3-17:	Maximum flow velocity for 1:500-year return period event 2120 sea level scenario – 1.06 m sea level rise - Head of the Bay.	26
Figure 3-18:	Maximum flow velocity for 1:500-year return period event 2120 sea level scenario – 1.06 m sea level rise - Lyttelton and Diamond Harbour.	27
Figure 3-19:	Maximum shear stress for 1:500-year return period event current sea level - Head of the Bay.	28
Figure 3-20:	Maximum shear stress for 1:500-year return period event current sea level - Lyttelton and Diamond Harbour.	28

Figure 3-21:	Maximum shear stress for 1:500-year return period event 2065 sea level scenario – 0.41 m sea level rise - Head of the Bay.	29
Figure 3-22:	Maximum shear stress for 1:500-year return period event 2065 sea level scenario – 0.41 m sea level rise - Lyttelton and Diamond Harbour.	29
Figure 3-23:	Maximum shear stress for 1:500-year return period event 2120 sea level scenario – 1.06 m sea level rise - Head of the Bay.	30
Figure 3-24:	Maximum shear stress for 1:500-year return period event 2120 sea level scenario – 1.06 m sea level rise - Lyttelton and Diamond Harbour.	30
Figure 3-25:	Tsunami water level at Wainui for the three sea level scenarios.	31
Figure 3-26:	Tsunami water level at Duvauchelle Bay entrance for the three sea level scenarios.	32
Figure 3-27:	Maximum inundation depth (i.e., height above ground) for 1:500-year return period event current sea level - Wainui and Akaroa.	32
Figure 3-28:	Maximum inundation depth (i.e., height above ground) for 1:500-year return period event current sea level – Upper Akaroa Harbour.	33
Figure 3-29:	Maximum inundation depth (i.e., height above ground) for 1:500-year return period event - 2065 sea level scenario – 0.41 m sea level rise - Wainui and Akaroa.	33
Figure 3-30:	Maximum inundation depth (i.e., height above ground) for 1:500-year return period event - 2065 sea level scenario – 0.41 m sea level rise - Upper Akaroa Harbour.	34
Figure 3-31:	Maximum inundation depth (i.e., height above ground) for 1:500-year return period event - 2120 sea level scenario – 1.06 m sea level rise - Wainui and Akaroa.	35
Figure 3-32:	Maximum inundation depth (i.e., height above ground) for 1:500-year return period event - 2120 sea level scenario – 1.06 m sea level rise - Upper Akaroa Harbour.	35
Figure 3-33:	Flow velocity at Wainui for the three sea level scenarios.	36
Figure 3-34:	Flow velocity at Duvauchelle Bay entrance for the three sea level scenarios.	37
Figure 3-35:	Maximum flow velocity for 1:500-year return period event current sea level - Wainui and Akaroa.	37
Figure 3-36:	Maximum flow velocity for 1:500-year return period event current sea level - Upper Akaroa Harbour.	38
Figure 3-37:	Maximum flow velocity for 1:500-year return period event 2065 sea level scenario – 0.41 m sea level rise - Wainui and Akaroa.	38
Figure 3-38:	Maximum flow velocity for 1:500-year return period event 2065 sea level scenario – 0.41 m sea level rise - Upper Akaroa Harbour.	39
Figure 3-39:	Maximum flow velocity for 1:500-year return period event 2120 sea level scenario – 1.06 m sea level rise - Wainui and Akaroa.	39
Figure 3-40:	Maximum flow velocity for 1:500-year return period event 2120 sea level scenario – 1.06 m sea level rise - Upper Akaroa Harbour.	40
Figure 3-41:	Maximum shear stress for 1:500-year return period event current sea level - Wainui and Akaroa.	41
Figure 3-42:	Maximum shear stress for 1:500-year return period event current sea level - Upper Akaroa Harbour.	41
Figure 3-43:	Maximum shear stress for 1:500-year return period event 2065 sea level scenario – 0.41 m sea level rise - Wainui and Akaroa.	42

Figure 3-44:	Maximum shear stress for 1:500-year return period event 2065 sea level scenario – 0.41 m sea level rise - Upper Akaroa Harbour.	42
Figure 3-45:	Maximum shear stress for 1:500-year return period event 2120 sea level scenario – 1.06 m sea level rise - Wainui and Akaroa.	43
Figure 3-46:	Maximum shear stress for 1:500-year return period event 2120 sea level scenario – 1.06 m sea level rise - Upper Akaroa Harbour.	43
Figure 6-1:	Tsunami inundation terminology.	47

Executive summary

NIWA has previously completed tsunami inundation modelling of 1:500-year and 1:2,500-year events for Christchurch City (from Taylor's Mistake in the south through to the Waimakariri River in the north) as part of the Land Drainage Recovery Programme (LDRP) Tsunami Study (Bosselle et al. 2018). This study adds to this previous modelling to better understand the tsunami hazard in Lyttelton and Akaroa Harbours, in order to have consistent tsunami inundation maps over the whole area.

This study simulates the tsunami inundation in Lyttelton and Akaroa Harbours for a 1:500-year tsunami event produced by a Mw 9.28 earthquake occurring in South Peru (same event as in the previous study) for three sea level conditions: 1) Mean High Water Spring (MHWS) at present mean sea level (MSL); 2) MHWS for 2065 MSL (0.41 m above present MSL); and 3) MHWS for 2120 MSL (1.06 m above present MSL). This study also evaluates the flow velocities associated with the tsunami waves and identifies the erosion potential using bottom shear stress as a proxy for sediment transport.

Results indicate that, in Lyttelton Harbour, Lyttelton Port, Purau and Charteris Bay are the most affected by the tsunami but inundation also occurs in the Head of the Bay and Governors Bay. Tsunami amplification at the Head of the Bay leads to inundation extending 2.5 km inland, with inundation depth exceeding 7 m.

In Akaroa Harbour, most bays are inundated by the tsunami, with more properties and residences exposed than in Lyttelton Harbour. Although not as severe as in the Head of the Bay in Lyttelton Harbour, the inundation extent and depth exceeds 300 m and 4 m in Akaroa town, respectively, as well as in most bays in the harbour.

The scenarios with increased sea levels result in an increase in the inundation depth and extent, and expose many more properties and residences in Akaroa Harbour (especially Akaroa town) to inundation and damage. Similar increases in tsunami depth and inundation did not significantly expose more properties in Lyttelton Harbour.

1 Introduction

NIWA has completed inundation modelling of the impact of a 1:500-year and a 1:2,500-year tsunami event on Christchurch City (from Taylor's Mistake in the south through to the Waimakariri River in the north). This work was conducted for Christchurch City Council (CCC) as part of the Land Drainage Recovery Programme (LDRP) Tsunami Study (Bosserelle et al. 2018). The CCC's purview covers a wider geographic region encompassing Lyttelton Harbour and Banks Peninsula. As such CCC are also interested in understanding the tsunami hazard in this wider region, especially in Lyttelton and Akaroa harbours, in order to have consistent tsunami inundation maps over the whole area for use in planning purpose. See Figure 6-1 and Page 47 for definitions of tsunami inundation terms used in this report.

This study simulates the tsunami inundation in Lyttelton and Akaroa Harbours for the same 1:500-year event as in the previous study for three sea level conditions (as calculated by Tonkin & Taylor (2017)): 1) Mean High Water Spring (MHWS) at present mean sea level (MSL); 2) MHWS for 2065 MSL (0.41 m above present MSL); and 3) MHWS for 2120 MSL (1.06 m above present MSL). This study also evaluates the flow velocities associated with the tsunami and identifies the erosion potential using bottom shear stress as a proxy for sediment transport (e.g., Powell 1998).

1.1 Use of this report

Whilst information provided in this report are intended to inform about the tsunami hazards, they may also be useful for strategic development and infrastructure planning as it may, when used with other hazard and risk information, highlight areas of higher vulnerability that are potentially unsuitable for future development. Digital GIS files and maps of the inundation extents should not be used at scales finer than 1:25,000. The overview maps are intended as a guide only and should not be used for interpreting inundation.

The main purpose of this report is to provide CCC with a clearer understanding of the potential 1:500-year tsunami inundation extent and the effects of sea-level rise on Lyttelton and Akaroa Harbours. The information provided is intended to aid understanding of the tsunami for current conditions and sea-level rise scenarios up to 2120 (1.06 m), including how tsunamis could impact the local bays in terms of geomorphic changes, scouring and deposition and resulting long-term effects.

1.2 Caveat

This report is based on state-of-the-art knowledge and modelling capabilities of tsunamis and tsunami inundation at the time of writing. While every effort was made to provide accurate information, there are many uncertainties involved including knowledge of potential tsunami sources, source characteristics, bathymetry and topography. In addition, while the hydrodynamic models capture much of the physics involved in tsunami propagation and inundation, they also include some simplifying assumptions, as with all models.

This report also provides a qualitative assessment of the potential erosion caused by the tsunami. This assessment is based on the model prediction of maximum shear stress which is only a proxy for sediment transport potential. As a result, no estimates can be made of the amount of erosion or the depth of scouring.

The information provided in this report is of a technical nature and should be considered with the above limitations in mind.

2 Methods

2.1 Models

The tsunami modelling was undertaken using ComMIT for Trans-Pacific tsunami propagation and Basilisk for the harbour simulation.

ComMIT stands for COMMunity Model Interface for Tsunami, and is an interface around NOAA's Method of Splitting Tsunamis (MOST) tsunami model (Titov et al. 2011). It uses initial conditions from the pre-computed propagation database SIFT (Short-term Inundation Forecast for Tsunamis database (Gica et al. 2008)).

Basilisk (Popinet 2015) is a partial differential equation solver based on adaptive Cartesian meshes that has been used for tsunami modelling in a range of situations (Lane et al. 2017, Lee et al. 2015, Popinet 2011, 2012).

In this study we follow the methodology of Bosserelle et al. (2018), where ComMIT is used to produce tsunami water levels near the coast at the boundary of the Basilisk model grid. Water levels simulated using ComMIT were then "nested" (i.e., used as a boundary forcing) in Basilisk for simulating tsunami propagation and inundation in Lyttelton and Akaroa Harbours.

2.2 Tsunami source

The aim of this work is to simulate the inundation from a tsunami generated by an earthquake on the South American subduction zone. Using a sensitivity analysis of tsunami wave heights in Pegasus Bay, Bosserelle et al. (2018) previously identified the fault segments from the SIFT database that would produce the largest waves in Pegasus Bay, namely, segments cs68z, cs69z and cs70z (Figure 2-1). While these faults are likely to produce large waves in Akaroa and Lyttelton Harbours, they may not necessarily be the fault segments that produce the largest waves in either harbour. In fact, Borrero and Goring (2015) showed, using a similar method, that the fault segments that produce the largest waves in Lyttelton Port for Mw 8.5 earthquake in South America are located between 25° and 30°S. However, because this study is following up from the work of Bosserelle et al. (2018) and to remain consistent with this previous study, the same tsunami source for the 1:500-year event is used. The event consists of a M_w 9.28 earthquake involving 13 SIFT fault segments (Figure 2-2) and a uniform slip of 35.89 m along each segment. The default SIFT rigidity of $4.4 \times 10^{11} \text{ dyn/cm}^2$ was assumed as is the case in Bosserelle et al. (2018). This was identified in the Probabilistic Tsunami Hazard Assessment undertaken in Power (2013) as being the most likely source scenario for the 1:500-year event (50th percentile) for Christchurch City.

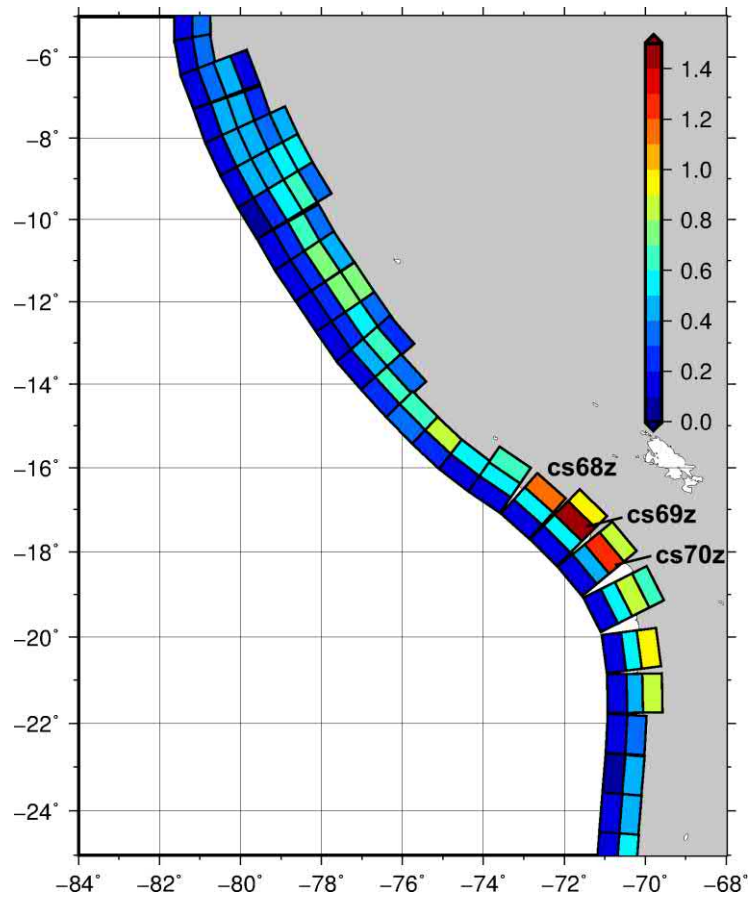


Figure 2-1: Maximum wave height in Pegasus Bay resulting from a 20m slip earthquake applied at each fault unit in the SIFT database for South America. Source: Bosserelle et al. (2018).

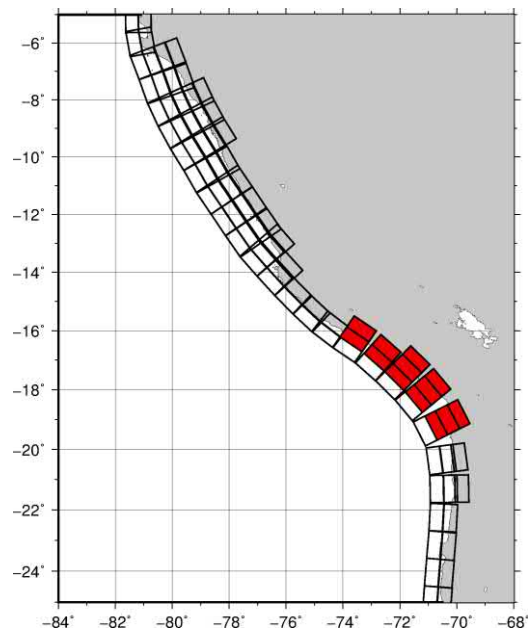


Figure 2-2: Fault segments involved in the Mw 9.28 earthquake scenario for 1:500-year tsunami inundation (highlighted in red). SIFT segments used are: cs67a, cs67z, cs68a, cs68z, cs69a, cs69y, cs69z, cs70a, cs70y, cs70z, cs71a, cs71y, cs71z. Source: Bosserelle et al. (2018).

2.3 Trans-Pacific Tsunami Propagation

In order to assess the inundation in both harbours, the tsunami wave had to be simulated from the source to the inundation model boundaries across the Pacific Ocean. This was done using the ComMIT interface which provides access to the propagation database for all of the SIFT faults (Figure 2-3). ComMIT was used with three grids of increasing resolution to the North and South of Banks Peninsula (Figure 2-4). The water levels extracted from the ComMIT simulation were then nested to the Basilisk grid to simulate the tsunami in each harbour (e.g., Figure 2-5).

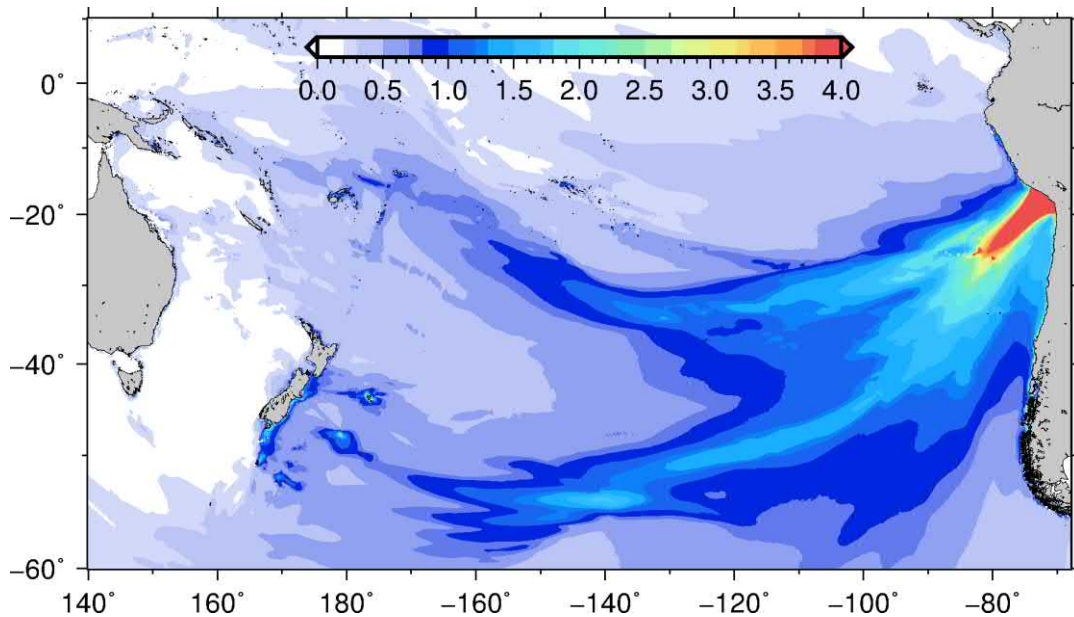


Figure 2-3: Maximum water level for the 1:500-year tsunami event trans-Pacific propagation.

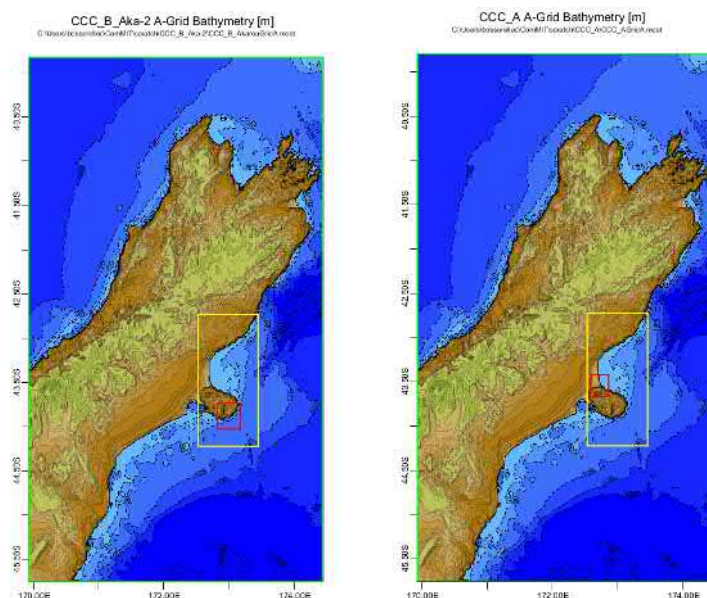


Figure 2-4: Nested grid extents used in ComMIT to propagate the tsunami waves to the Basilisk boundaries. Akaroa ComMIT grids layout on the left and Lyttelton on the right. The A-grid is the extent of the figure, the B-grid is in the yellow rectangle and the C-grid in the red rectangle. A and B grids were the same for both Lyttelton and Akaroa harbours.

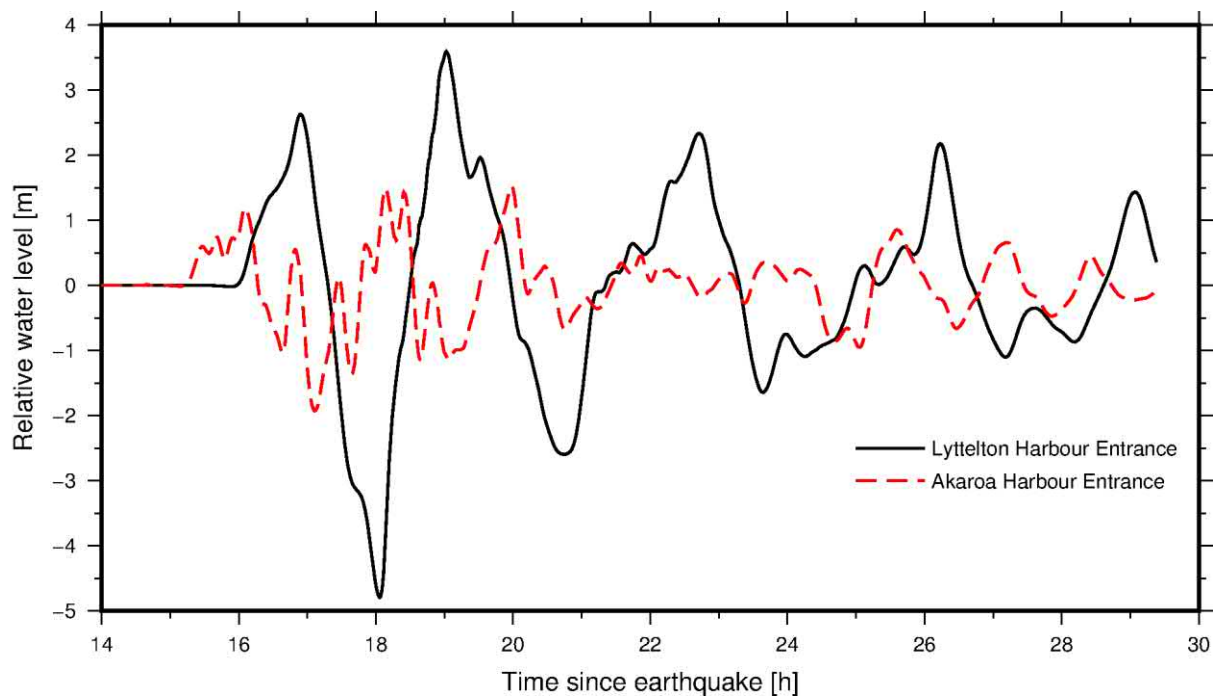


Figure 2-5: Water levels at the entrance of Lyttelton and Akaroa harbours as simulated using ComMIT.

2.4 Local bathymetry/topography

The Basilisk model topography/bathymetry grids were created by collating available topography and bathymetry data sourced from LiDAR and bathymetry surveys, as well as nautical charts information. The data sources were all shifted to the Lyttelton Vertical Datum (LVD37) equivalent to MSL and then interpolated to a 10 m grid.

2.4.1 Lyttelton Harbour

For Lyttelton, 2008 and 2015 LiDAR datasets were available for most of the shore of the harbour. The 2008 dataset was used to complement the extent of the 2015 survey in low lying areas. Bathymetry data collected by Hart et al. (2008) was used in most of the upper harbour while the LINZ chart data (NZ 6321) was used in the lower part of the harbour and a single beam survey for the main entrance channel (MGD77-557371) (Figure 2-6). In several areas, the LINZ chart contours or soundings were removed because they were inconsistent with the survey from Hart et al. (2008). Similarly, some line survey data from Hart et al. (2008) were removed as they were either inconsistent with other lines of the same survey, or inconsistent with data from the LiDAR survey.

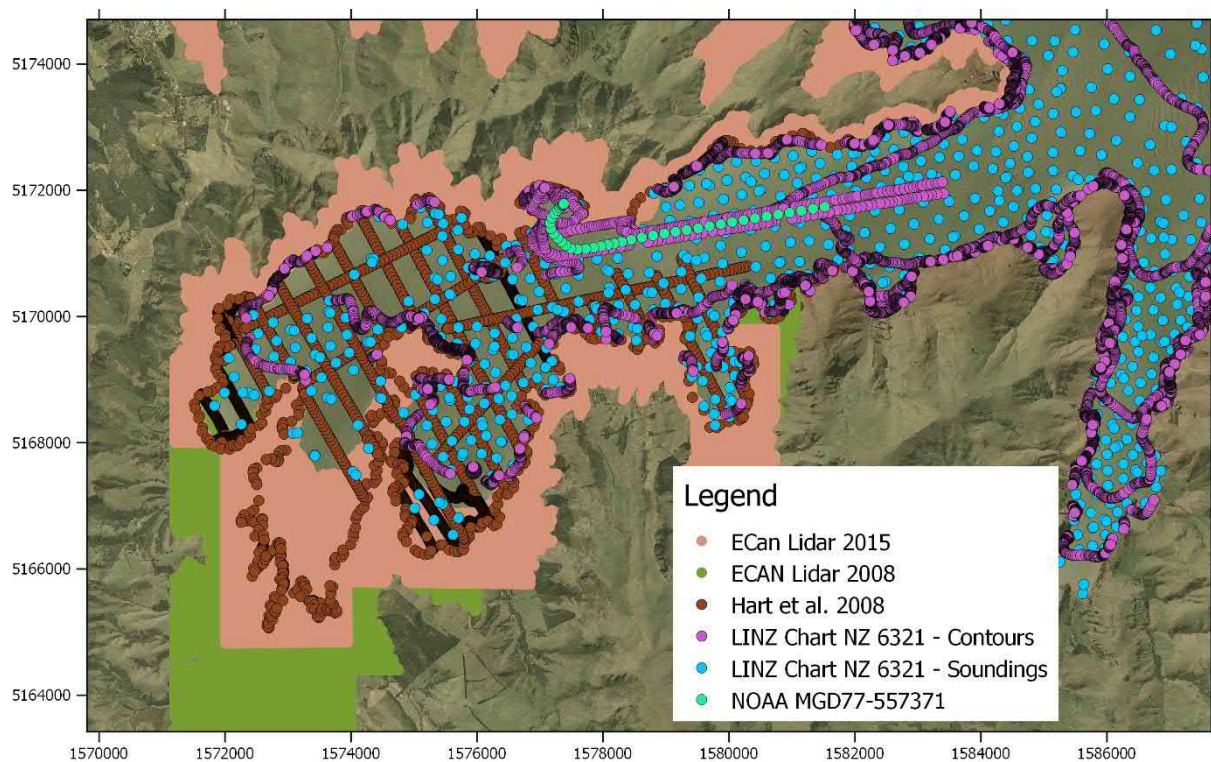


Figure 2-6: Bathymetry and topography data collated to produce the Lyttelton model grid.

The datasets were combined and gridded with at 10 m resolution using a continuous curvature spline in tension (Smith and Wessel 1990). The gridded bathymetry was then rotated 40° clockwise so that the model's boundary on the right would be parallel to the harbour entrance (Figure 2-7).

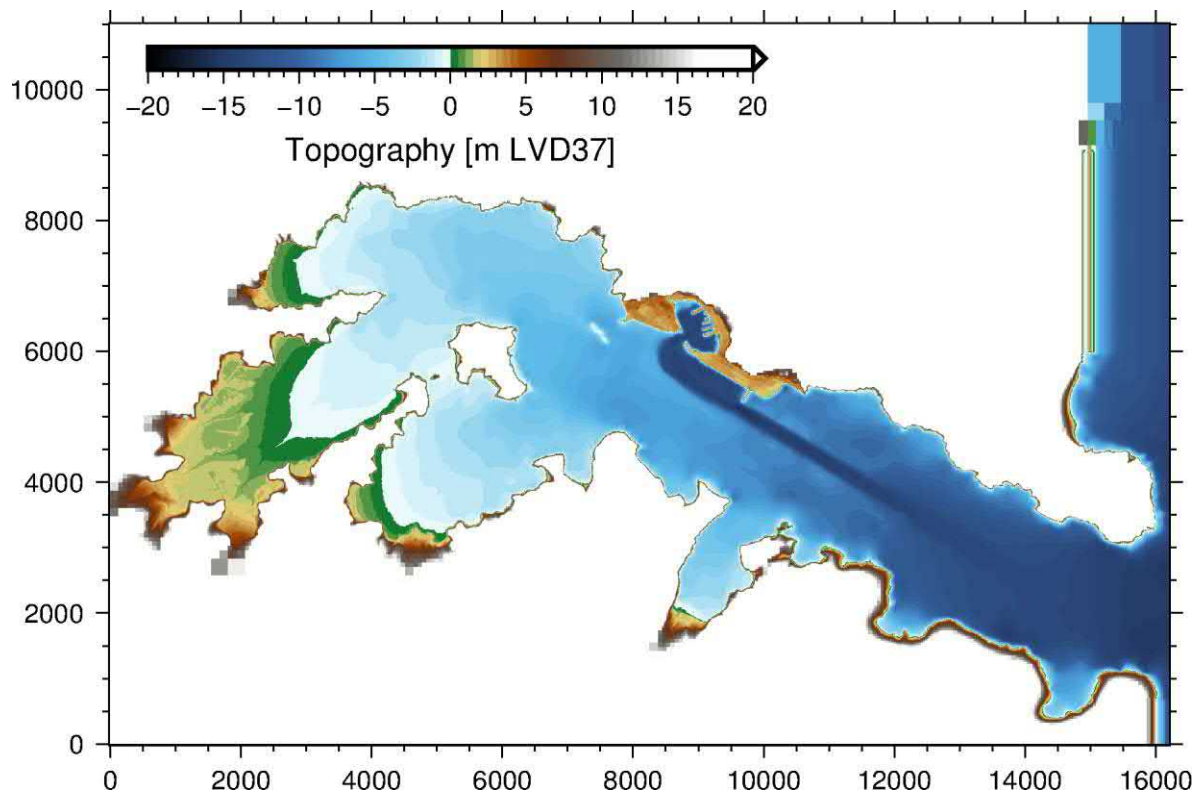


Figure 2-7: Lyttelton Harbour bathymetry grid as used in the Basilisk model.

2.4.2 Akaroa Harbour

For Akaroa, the 2008 LiDAR data covered the shores of the upper half of the harbour. The bathymetry data collected by Hart et al. (2009) was used in most of the harbour while the LINZ chart data (NZ 6324) was used in the harbour entrance. Other parts of Banks Peninsula were extracted from the NIWA 205m New Zealand bathymetry (Figure 2-8).

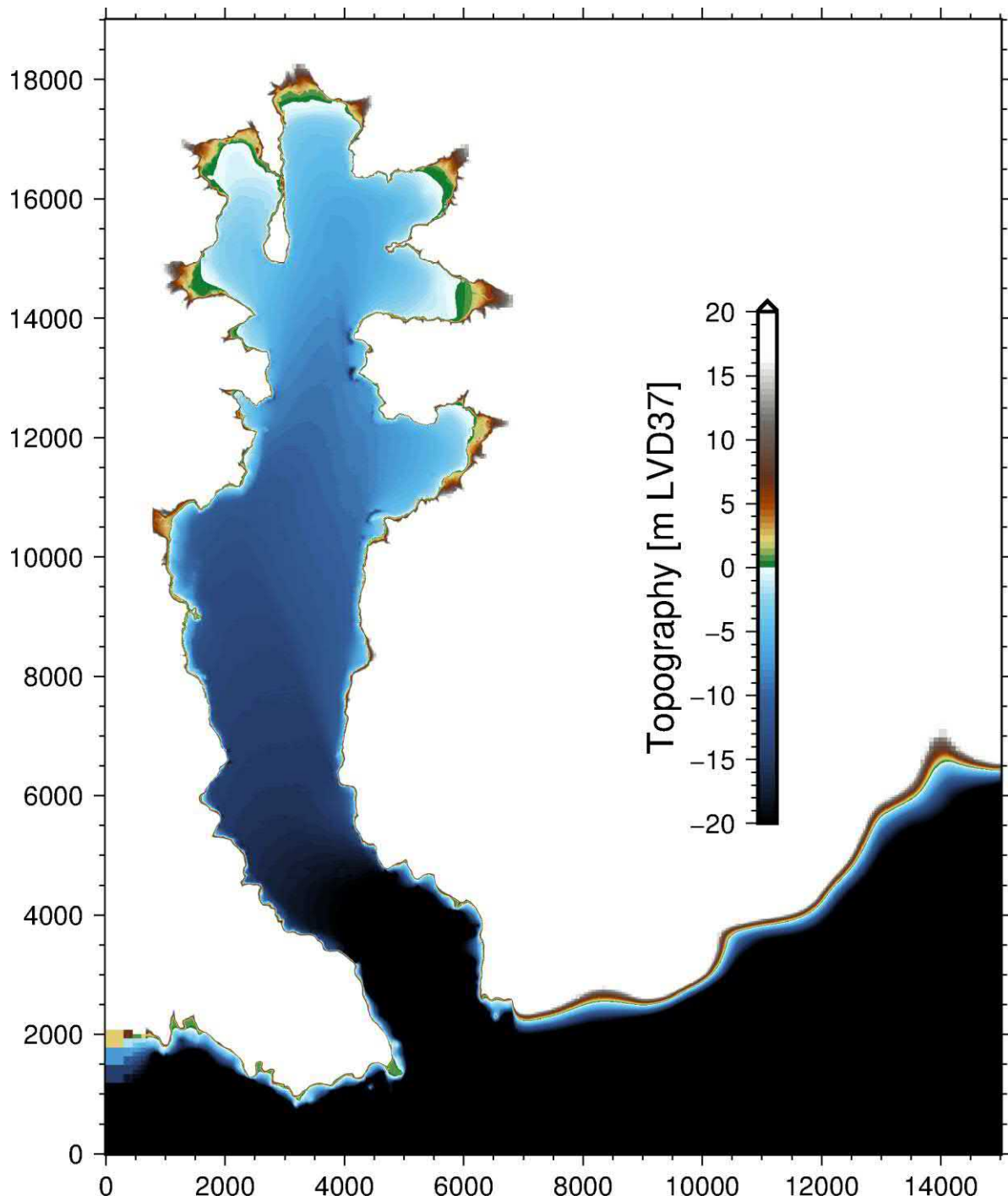


Figure 2-8: Akaroa Harbour bathymetry grid as used in the Basilisk model.

2.5 Erosion evaluation

The erosion potential is described by the flow bottom shear stress (Powell 1998). This allows for a qualitative assessment of the locations where scouring is most likely to occur for each scenario using information of maximum bottom shear-stress, maximum flow velocity and maximum inundation depth. This is done on a broad scale and does not capture smaller scale scouring that may occur around buildings, small-scale structures (e.g., bridges, culverts) or small-scale channels (e.g., streams).

The critical shear stress is the minimum shear stress necessary to mobilise a particle of sediment of a given size (Table 2-1). In Lyttelton Harbour, fine sediment (silt and clay) dominate the upper harbour (Hart et al. 2008). In Akaroa the seabed is mostly muddy coarsening to sand at the harbour entrance. Pockets of sand also occur on the tidal flats at the head of the bays (Hart et al. 2009).

Table 2-1: Critical shear stress by particle-size classification for determining approximate condition for sediment. Note that critical shear stress only indicates mobility rather than transport. This table was calculated using a fixed sediment density. From Berenbrock and Tranmer (2008).

Particle classification name	Ranges of particle diameters	Critical bed shear stress (τ_c) (N/m ²)
Coarse cobble	128 – 256	112 – 223
Fine cobble	64 – 128	53.8 – 112
Very coarse gravel	32 – 64	25.9 – 53.8
Coarse gravel	16 – 32	12.2 – 25.9
Medium gravel	8 – 16	5.7 – 12.2
Fine gravel	4 – 8	2.7 – 5.7
Very fine gravel	2 – 4	1.3 – 2.7
Very coarse sand	1 – 2	0.47 – 1.3
Coarse sand	0.5 – 1	0.27 – 0.47
Medium sand	0.25 – 0.5	0.194 – 0.27
Fine sand	0.125 – 0.25	0.145 – 0.194
Very fine sand	0.0625 – 0.125	0.110 – 0.145
Coarse silt	0.0310 – 0.0625	0.0826 – 0.110
Medium silt	0.0156 – 0.0310	0.0630 – 0.0826
Fine silt	0.0078 – 0.0156	0.0378 – 0.0630

2.6 Validation

The tide gauges in Lyttelton Port have previously recorded several historical tsunami events (see Borrero and Goring 2015). The largest recorded tsunami at the Lyttelton tide gauge was the Valdivia tsunami in 1960 originating from Chile. Replicating this historical tsunami using the ComMIT and

Basilisk numerical models provides an opportunity to confirm the validity of the methodology used in this study.

The Valdivia earthquake that occurred on the 22 May 1960, was the most powerful earthquake ever recorded (Mw 9.5) and produced one of the most destructive tsunami in the Pacific. Even though the largest wave arrived in Lyttelton Harbour at low tide, the tsunami inundated paddocks at the head of the harbour (Scott 1963), and inundation of the Port caused damage to electrical gears (De Lange and Healy 1986). The tide gauge located in Lyttelton Port recorded the tsunami wave in great detail (Bell 2003), and can be used to evaluate the validity of the tsunami simulation used in this study.

The Valdivia tsunami wave in Pegasus Bay near the entrance of Lyttelton Harbour was obtained using the ComMIT interface and the same fault mechanism from Fujii and Satake (2013); which was adapted to the SIFT database by Borrero and Goring (2015).

In order to adequately compare the tsunami simulation methodology of this study and the record of the Valdivia tsunami, the Lyttelton gauge record was de-tided (i.e., the predicted tide was removed from the original record) and shifted to MHWS. The water level was extracted from the model at each time step for the approximate location of the tide gauge inside Lyttelton Port.

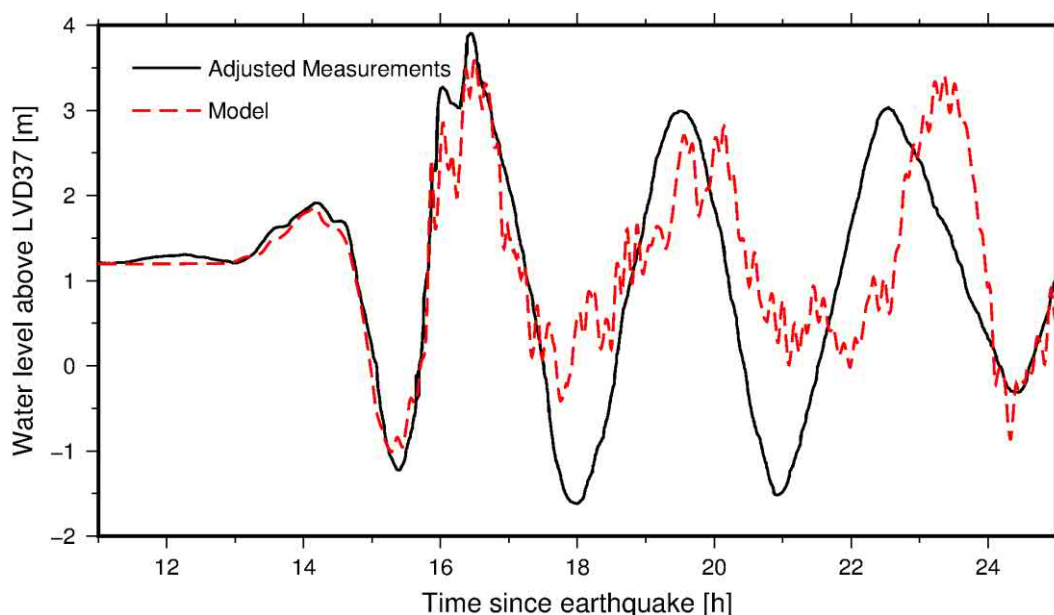


Figure 2-9: Model validation for the Valdivia tsunami of 1960. Note that the tidal component of the signal was removed from the Lyttelton gauge and the record was shifted to MHWS (1.2m above LVD37). The model time was shifted forward by 10 minutes to match with the arrival of the first wave.

The methodology used in this study when applied to the Valdivia event captures the height of the tsunami very well. The amplification of the wave in the harbour is well captured, the elevation of the tsunami is well captured and the timing of the second waves is good, but less so for the third and fourth waves (Figure 2-9). This could be due to a number of factors such as inaccuracies of the earthquake source, interaction between the tide and the tsunami wave (not included in this simulation), or changes in the harbour bathymetry since 1960. Nevertheless, this result confirms that the methodology produces accurate tsunami waves in Lyttelton Harbour.

3 Results

3.1 Lyttelton Harbour

3.1.1 Inundation for 2018

Lyttelton Harbour has a steep topography on the coast protecting most of the shoreline from tsunami waves. Low lying areas of the harbour that are exposed to tsunami inundation are the port site, Purau Bay, Charteris Bay, the Head of the Bay and Governors Bay.

Analysis of the inundation from the 1:500-year event occurring at MHWS for the present mean sea level indicates that the Head of the Bay shows the most extensive inundation reaching 1.5 km inland near Teddington. The inundation depth was also the highest at the Head of the Bay exceeding 7 m seaward of Teddington road on the western side of the bay (Figure 3-1).

Purau and Charteris Bay were also inundated with the inundation extending 300–400 m inland and with inundation depths exceeding 2.5 m.

The port site is heavily inundated with most of the site exceeding inundation depths of 2.5 m which would cause severe damage. Although not modelled in this study debris from the port (e.g., logs, shipping containers) could be spread throughout the harbour and significantly exacerbate tsunami damage. Because of its steep topography, Lyttelton township is not significantly inundated by the tsunami, with inundation reaching only a few properties on the town side of Norwich Quay (Figure 3-2) but Norwich Quay itself could be affected.

3.1.2 Effect of higher sea level scenario

As expected, the inundation extends further inland and inundation depth is greater with each increasing sea level scenario.

In the Port site, the maximum inundation depth up to 4.5 m for 2018 (MHWS), 5.4 m for 2065 (MMHWS+0.41) and 6.7 m for 2120 (MHWS+1.06 m). This difference is higher than expected from the increase in mean sea level, which suggests that the tsunami wave amplification is higher with higher sea level (Figure 3-3, Figure 3-7, Figure 3-9).

At the head of the Bay the amplification caused by higher sea level is also evident, with maximum inundation depths at Teddington Junction of 7.5 m for 2018(MSL), 8 m for 2065 (MSL+0.41) and 9.5 m for 2120(MSL+1.06 m) (Figure 3-4, Figure 3-6, Figure 3-8). The higher flow depth does not directly translate to much larger inundation extent as the inundation reaches slightly steeper topography and extends about 90 m further inland for both the 2065 and 2120 scenarios.

At the head of Charteris Bay, compared with the 2018 scenario, inundation extends a further 45 m inland for the 2065 scenario and a further 190 m inland for the 2120 scenario. Similarly, in Purau (Figure 3-5), the inundation extent reaches 100 m further inland in both the 2060 scenario and the 2120 scenario compared with the 2018 scenario. The similar inundation extent for 2065 and 2120 in Purau is because the inundation reaches steeper topography at the end of the bay, thus limiting the inundation extent. However, the inundation depths are affected by higher sea level with nearly 5 m for 2018(MSL), 5.8 m for 2065 (MSL+0.41) and 5.4 m for 2120 (MSL+1.06 m) Note that the maximum depth for the 2120 scenario is lower because some of the lower lying land in previous scenarios is now below high tide.

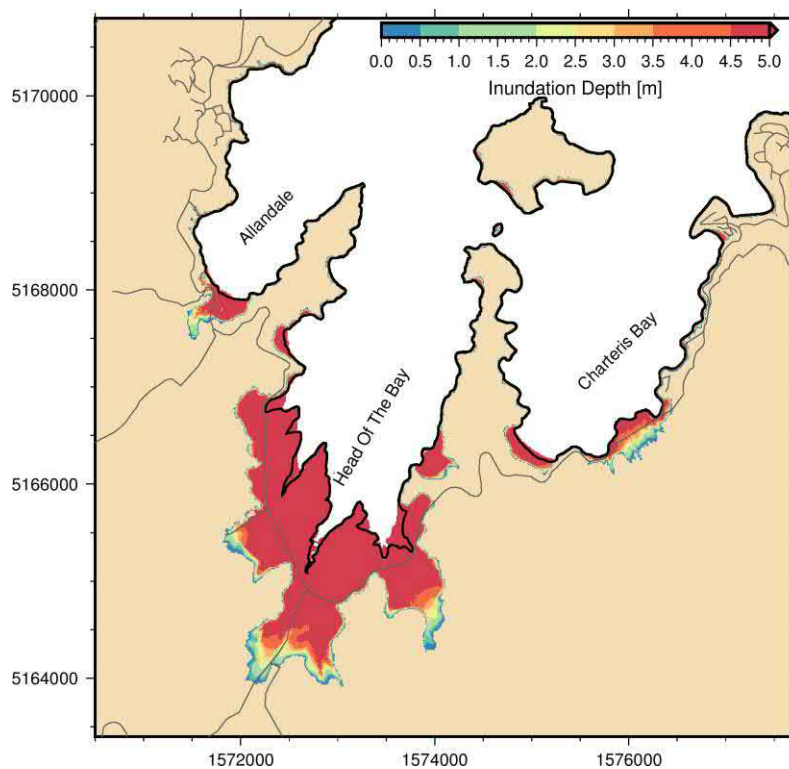


Figure 3-1: Maximum inundation depth (i.e., height above ground) for 1:500-year return period event current sea level - Head of the Bay.

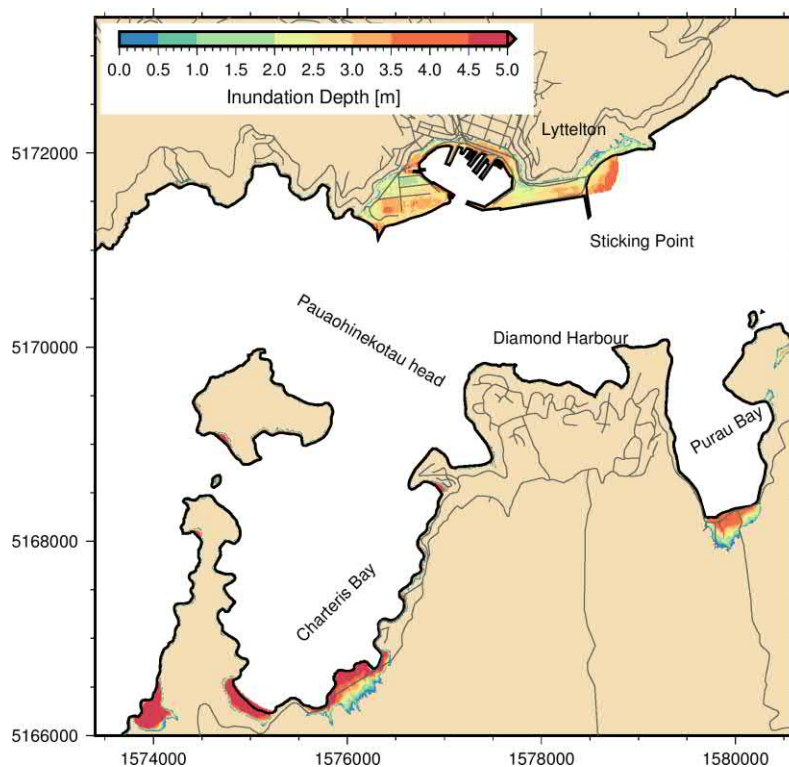


Figure 3-2: Maximum inundation depth (i.e., height above ground) for 1:500-year return period event current sea level – Lyttelton and Diamond Harbour. Note that the black coastline in the image does not include the reclamation that has occurred near Sticking Point.

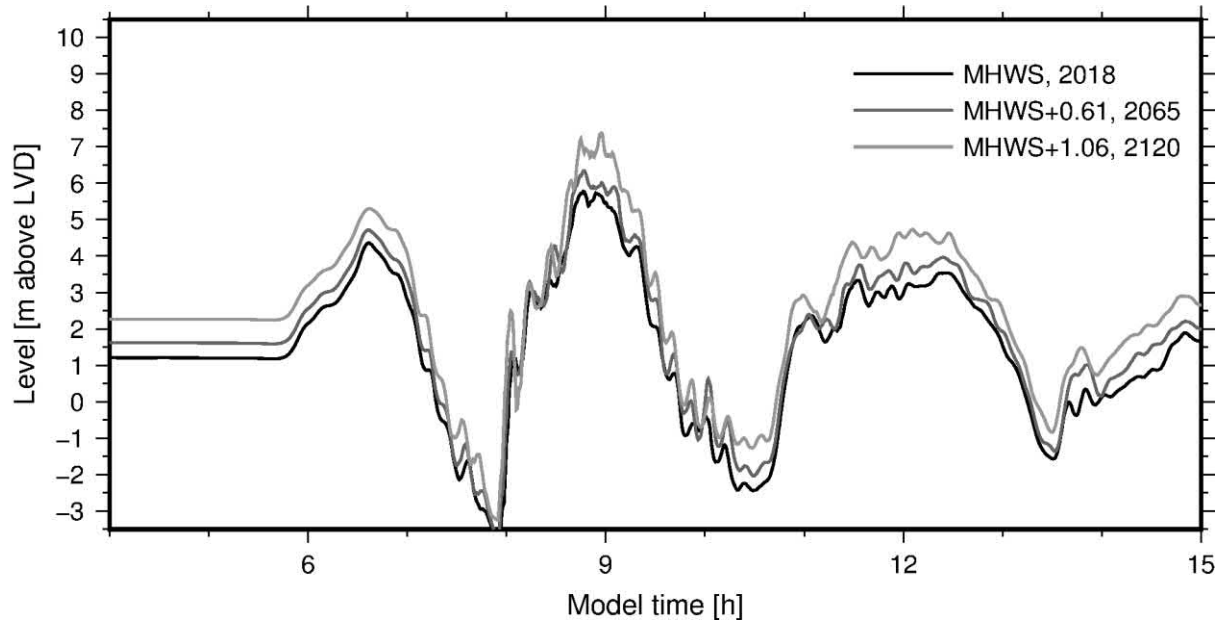


Figure 3-3: Tsunami water level at the Port entrance for the three sea level scenarios. The black line shows the tsunami at Mean High Water Spring (MHWS) at present mean sea level (MSL) scenario, the dark grey line shows the tsunami at MHWS for 2065 MSL (0.41 m above present MSL) scenario and the grey line shows the tsunami at MHWS for 2120 MSL (1.06 m above present MSL).

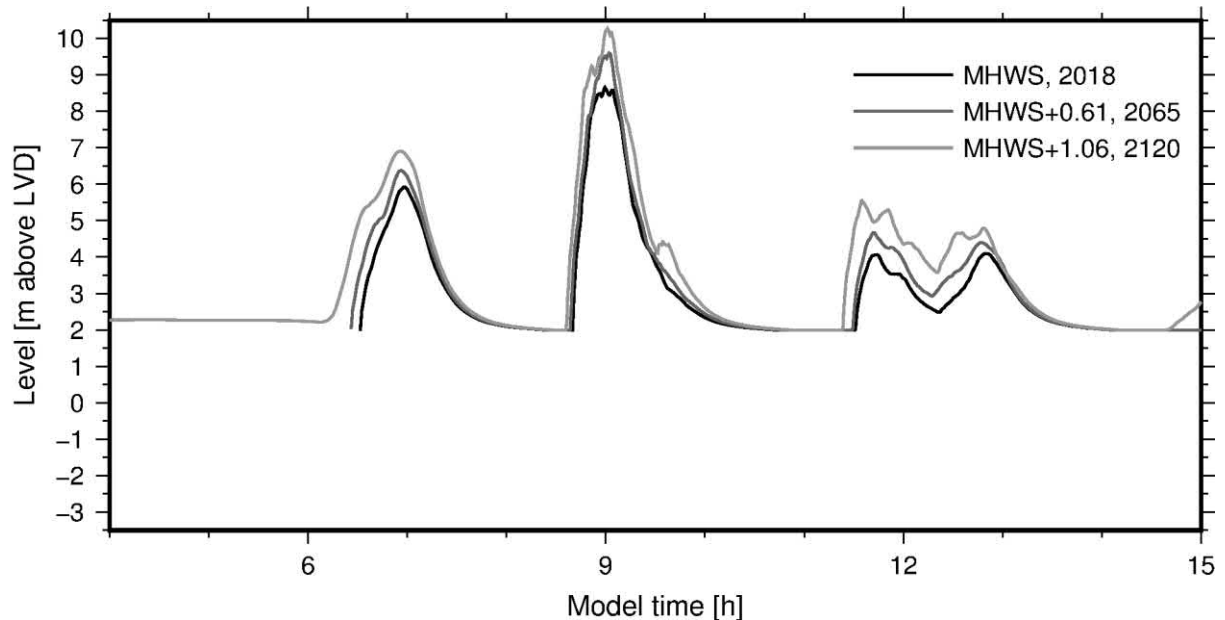


Figure 3-4: Tsunami water level at Teddington for the three sea level scenarios. The black line shows the tsunami at Mean High Water Spring (MHWS) at present mean sea level (MSL) scenario, the dark grey line shows the tsunami at MHWS for 2065 MSL (0.41 m above present MSL) scenario and the grey line shows the tsunami at MHWS for 2120 MSL (1.06 m above present MSL).

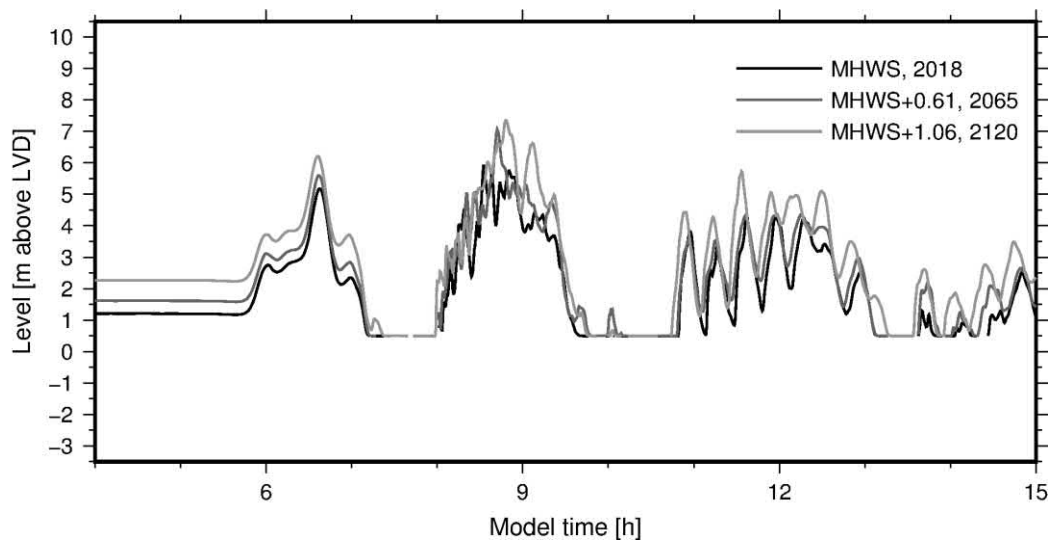


Figure 3-5: Tsunami water level at the head of Purau Bay for the three sea level scenarios. The black line shows the tsunami at Mean High Water Spring (MHWS) at present mean sea level (MSL) scenario, the dark grey line shows the tsunami at MHWS for 2065 MSL (0.41 m above present MSL) scenario and the grey line shows the tsunami at MHWS for 2120 MSL (1.06 m above present MSL).

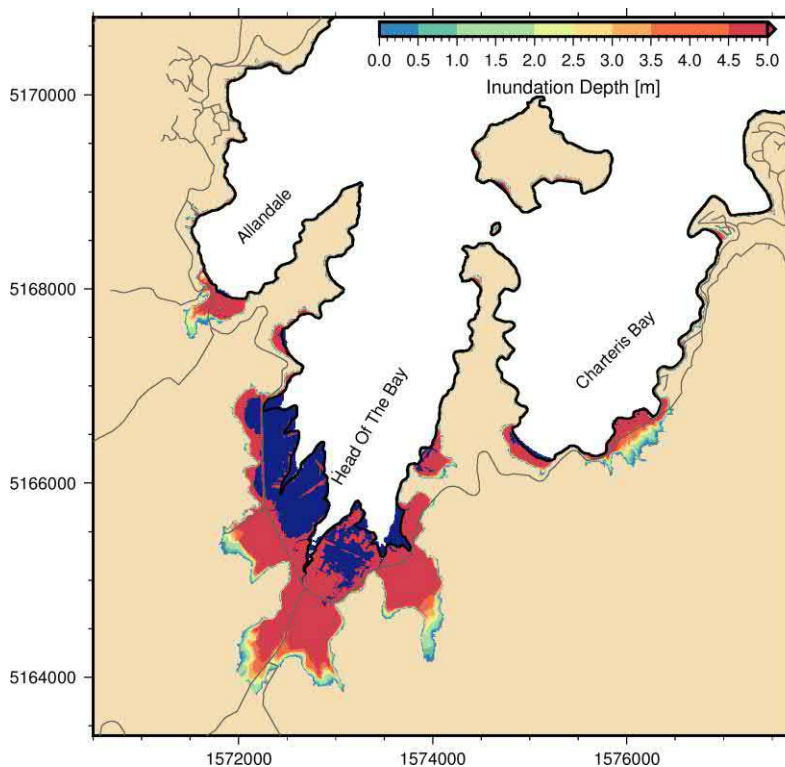


Figure 3-6: Maximum inundation depth (i.e., height above ground) for 1:500-year return period event - 2065 sea level scenario – 0.41 m sea level rise - Head of the Bay. Dark blue represents current land that will be below high tide in this sea level rise scenario. Erosional processes during the sea level rise may affect the position of the shoreline, this change is not taken into account here.

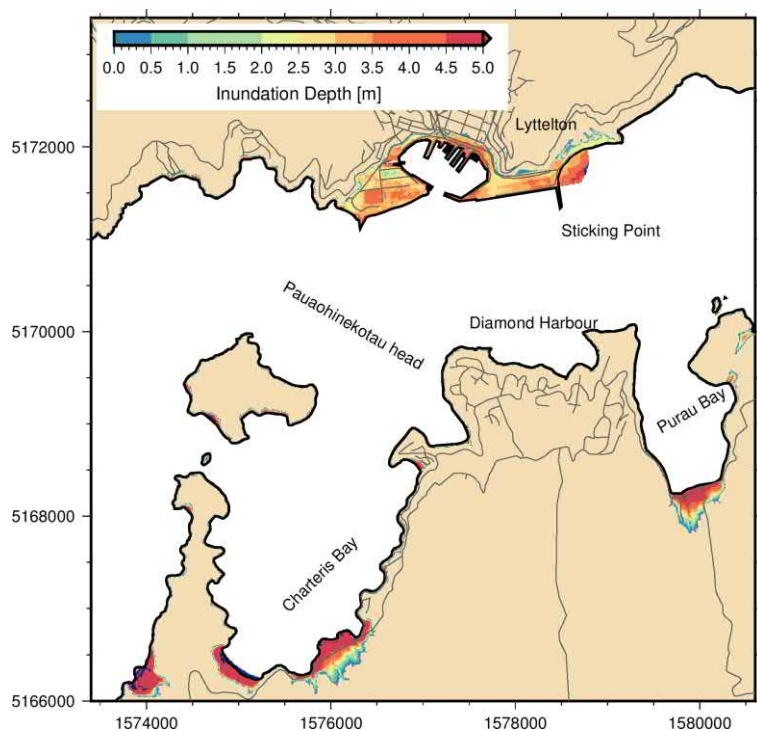


Figure 3-7: Maximum inundation depth (i.e., height above ground) for 1:500-year return period event - 2065 sea level scenario – 0.41 m sea level rise - Lyttelton and Diamond Harbour. Dark blue represents current land that will be below high tide in this sea level rise scenario. Erosional processes during the sea level rise may affect the position of the shoreline, this change is not taken into account here.

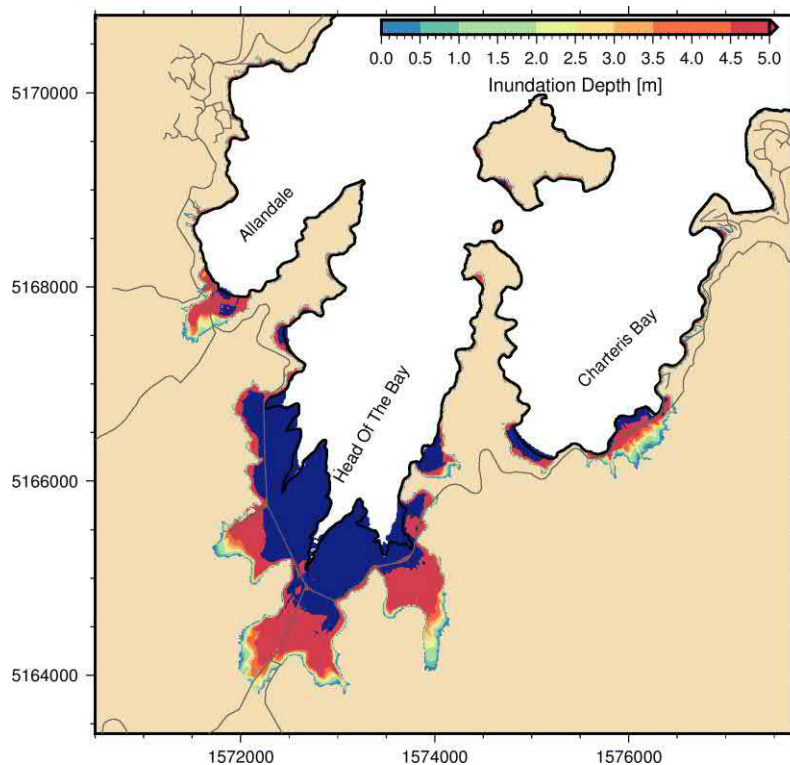


Figure 3-8: Maximum inundation depth (i.e., height above ground) for 1:500-year return period event - 2120 sea level scenario – 1.06 m sea level rise - Head of the Bay. Dark blue represents current land that

will be below high tide in this sea level rise scenario. Erosional processes during the sea level rise may affect the position of the shoreline, this change is not taken into account here.

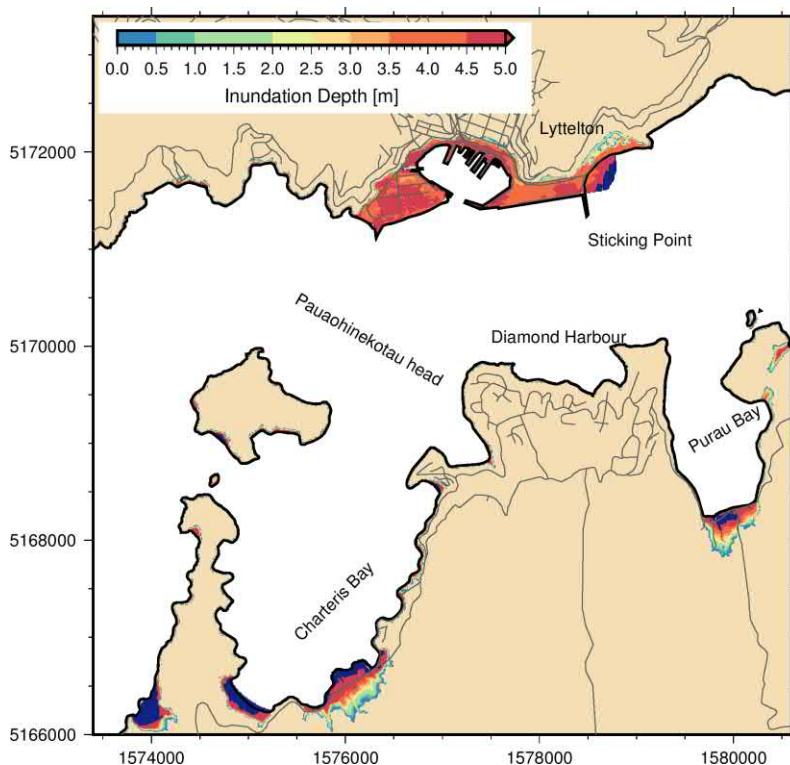


Figure 3-9: Maximum inundation depth (i.e., height above ground) for 1:500-year return period event - 2120 sea level scenario – 1.06 m sea level rise - Lyttelton and Diamond Harbour. Dark blue represents current land that will be below high tide in this sea level rise scenario. Erosional processes during the sea level rise may affect the position of the shoreline, this change is not taken into account here.

3.1.3 Maximum velocity

The tsunami simulation consists of four successive tsunami waves with a maximum amplitude (peak to trough) of 10 m. These waves successively flood and drain the head of the harbour creating strong currents and large eddies. For the 2018 sea level scenario, the largest velocities occur off diamond Harbour (Pauaohinekotau head) with velocities reaching close to 10 m/s, near Sticking Point (Figure 3-10, Figure 3-11) and South of Godley head. Such flow velocities are capable of causing severe damages to cables and pipelines crossing the Harbour (note that some pipelines and telecom cables were significantly damaged during the much smaller Maule tsunami in 2010).

Both higher sea level scenarios indicated faster flows in the main channels of the Harbour and at the entrance of the main bays. This is likely due to the higher water level in these scenarios, which means there is more water to drain in the Head of the Bay, and the greater depth of the harbour would allow faster flows due to a decrease in seafloor drag with depth (Figure 3-15–Figure 3-18).

Flow velocity in the inundated area is not significantly affected by higher sea level scenarios. At the Port entrance the maximum flow velocity is close to 5 m/s in all three scenarios (Figure 3-12). In Teddington the pattern of flow velocity is slightly modified in the different scenario but the maximum value remains identical close to 3.5 m/s (Figure 3-13). Similarly, in Purau the flow velocities are mostly identical in all three scenarios (Figure 3-14).

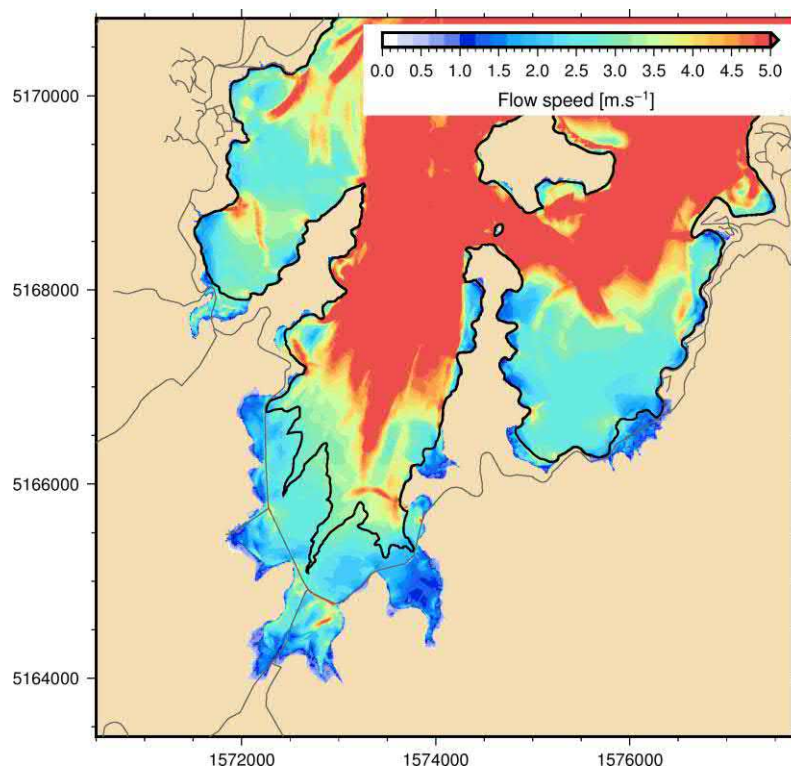


Figure 3-10: Maximum flow velocity for 1:500-year return period event current sea level - Head of the Bay.

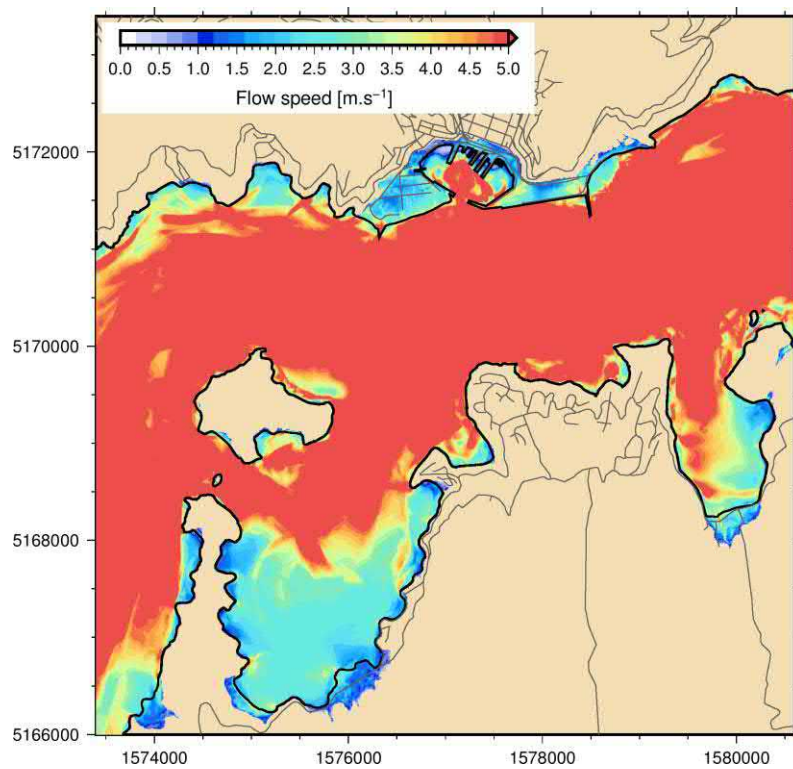


Figure 3-11: Maximum flow velocity for 1:500-year return period event current sea level - Lyttelton and Diamond Harbour.

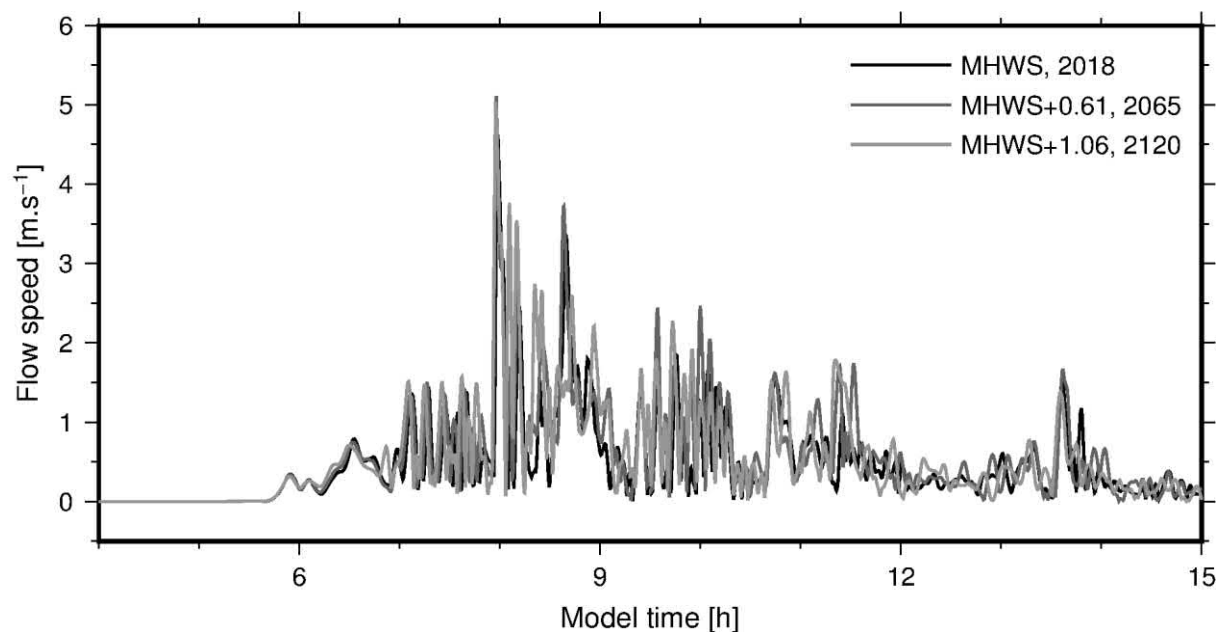


Figure 3-12: Flow velocity at the port entrance for the three sea level scenarios. The black line shows the tsunami at Mean High Water Spring (MHWS) at present mean sea level (MSL) scenario, the dark grey line shows the tsunami at MHWS for 2065 MSL (0.41 m above present MSL) scenario and the grey line shows the tsunami at MHWS for 2120 MSL (1.06 m above present MSL).

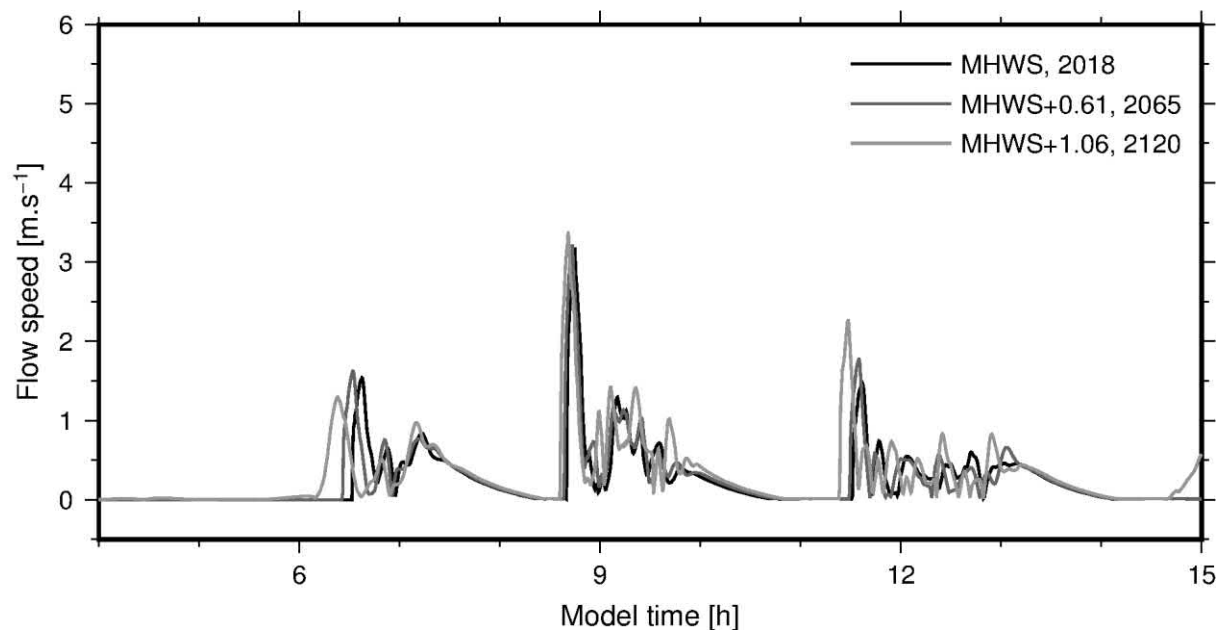


Figure 3-13: Flow velocity at Head of the Bay for the three sea level scenarios. The black line shows the tsunami at Mean High Water Spring (MHWS) at present mean sea level (MSL) scenario, the dark grey line shows the tsunami at MHWS for 2065 MSL (0.41 m above present MSL) scenario and the grey line shows the tsunami at MHWS for 2120 MSL (1.06 m above present MSL).

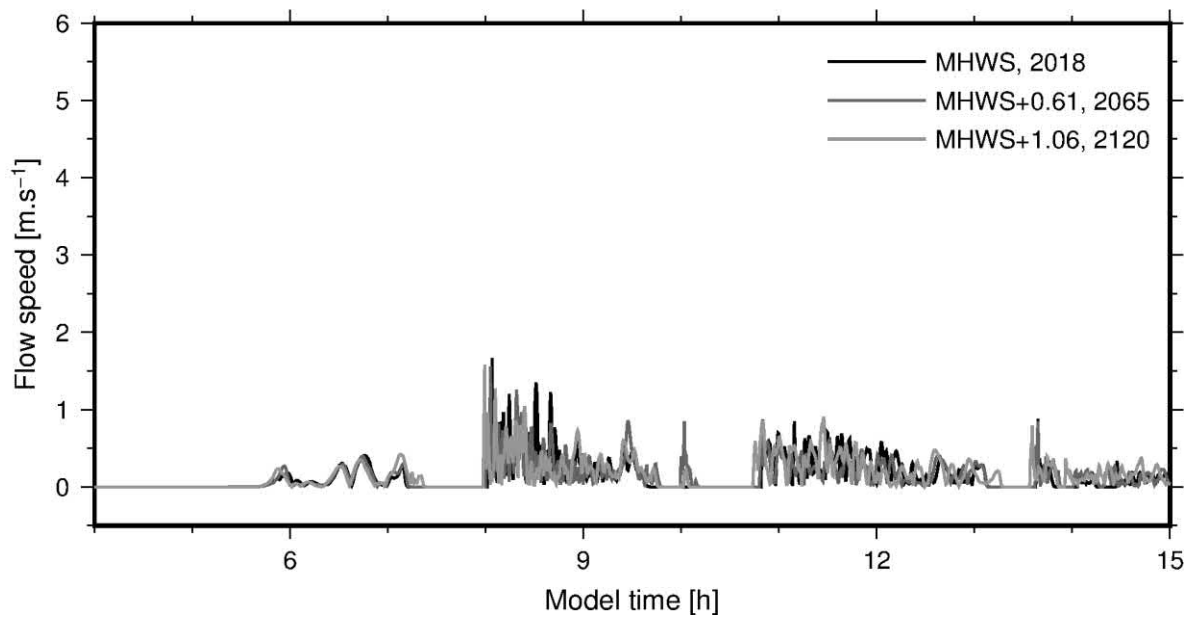


Figure 3-14: Flow velocity at the head of Purau Bay for the three sea level scenarios. The black line shows the tsunami at Mean High Water Spring (MHWS) at present mean sea level (MSL) scenario, the dark grey line shows the tsunami at MHWS for 2065 MSL (0.41 m above present MSL) scenario and the grey line shows the tsunami at MHWS for 2120 MSL (1.06 m above present MSL).

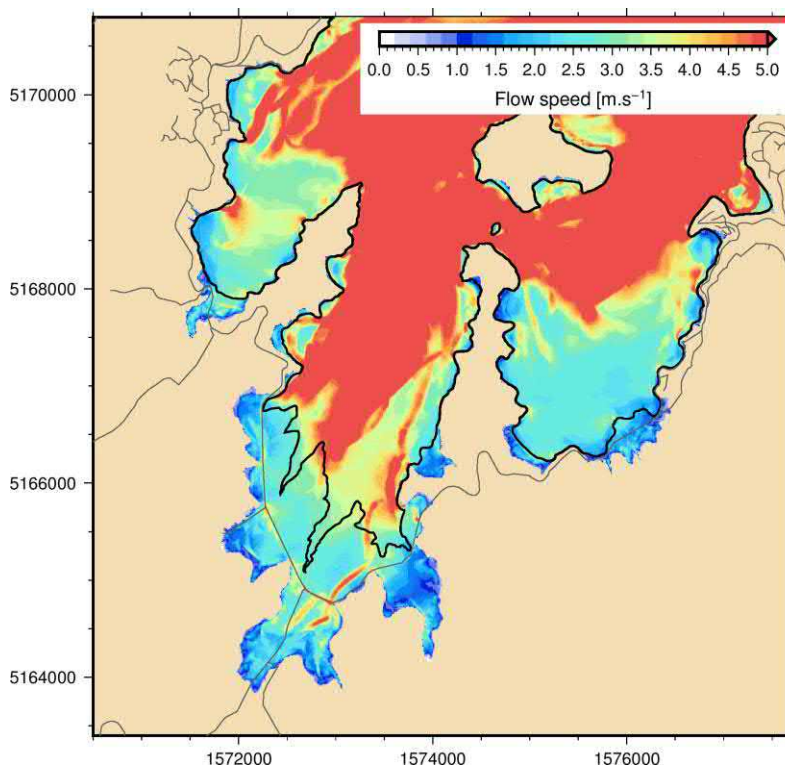


Figure 3-15: Maximum flow velocity for 1:500-year return period event 2065 sea level scenario – 0.41 m sea level rise - Head of the Bay.

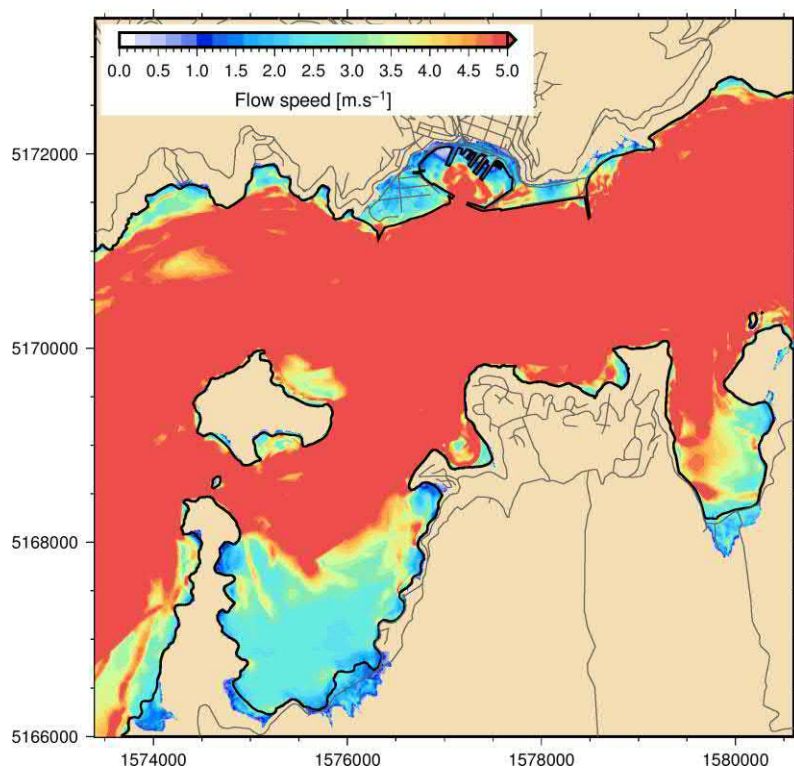


Figure 3-16: Maximum flow velocity for 1:500-year return period event 2065 sea level scenario – 0.41 m sea level rise - Lyttelton and Diamond Harbour.

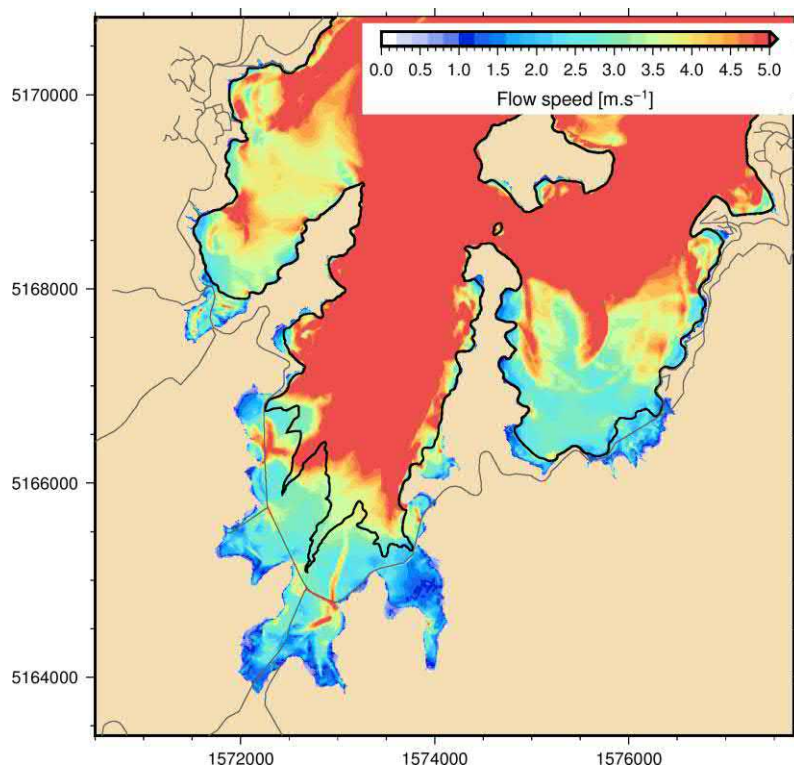


Figure 3-17: Maximum flow velocity for 1:500-year return period event 2120 sea level scenario – 1.06 m sea level rise - Head of the Bay.

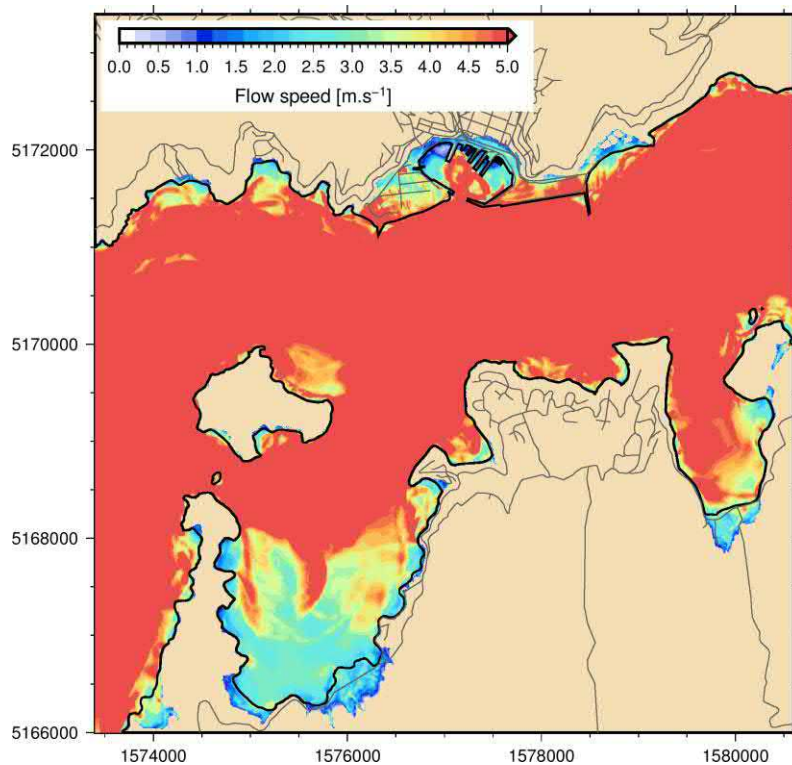


Figure 3-18: Maximum flow velocity for 1:500-year return period event 2120 sea level scenario – 1.06 m sea level rise - Lyttelton and Diamond Harbour.

3.1.4 Erosion potential

The maximum shear stress for the present sea level scenario significantly exceeds the critical shear stress necessary to transport the soft sediment present in the Harbour (Figure 3-19–Figure 3-24). It is likely that the eddies forming at the bay entrance are going to resuspend and transport sediment causing temporary morphological changes to the bathymetry by deepening channels and depositing coarser sediment where the current slows.

In Teddington the inundation occurs as a series of high waves that reaches the road with high velocities and high shear stress that are likely to cause some scouring near the road.

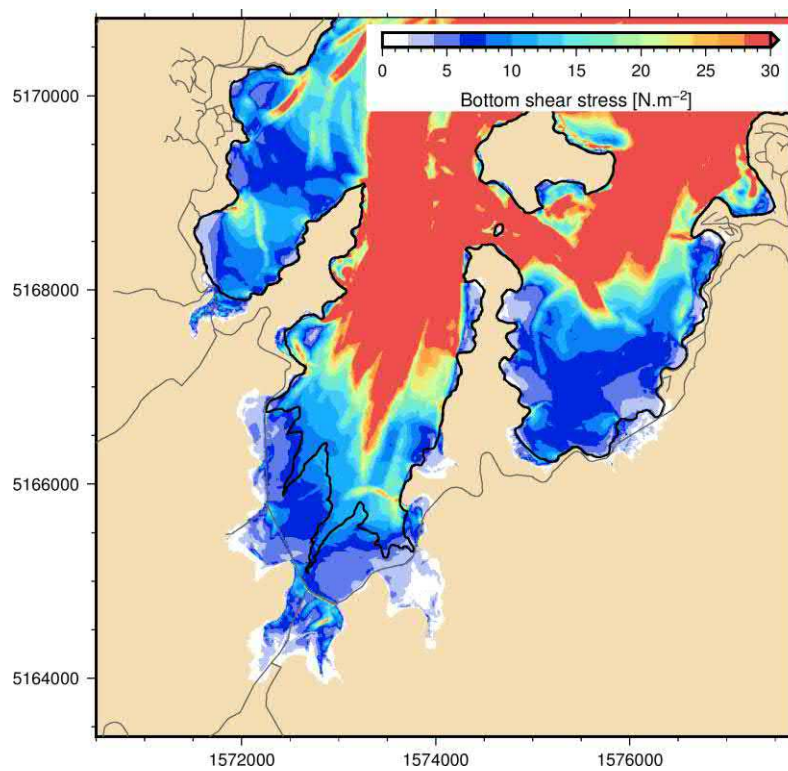


Figure 3-19: Maximum shear stress for 1:500-year return period event current sea level - Head of the Bay.

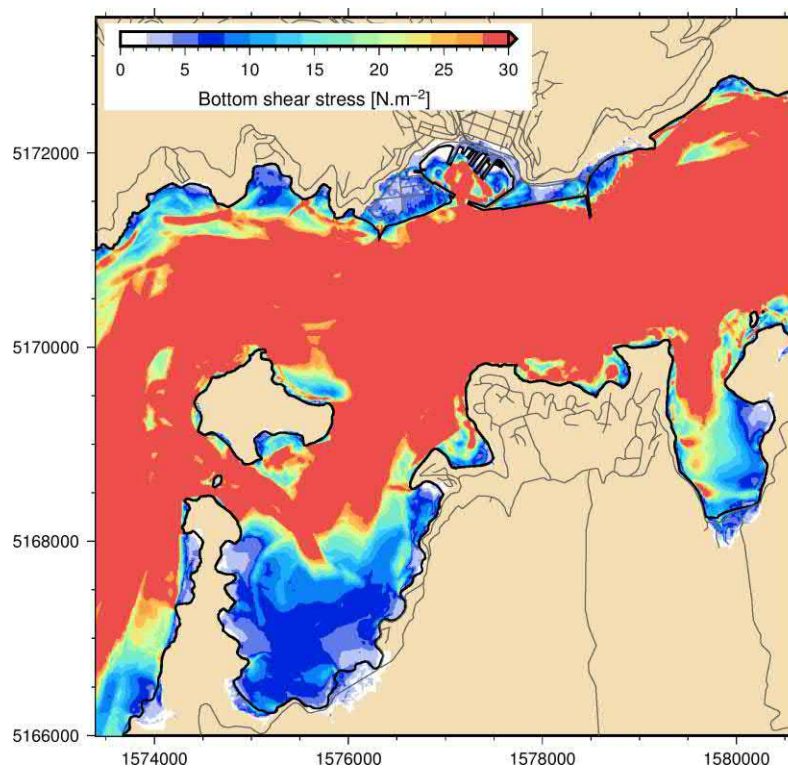


Figure 3-20: Maximum shear stress for 1:500-year return period event current sea level - Lyttelton and Diamond Harbour.

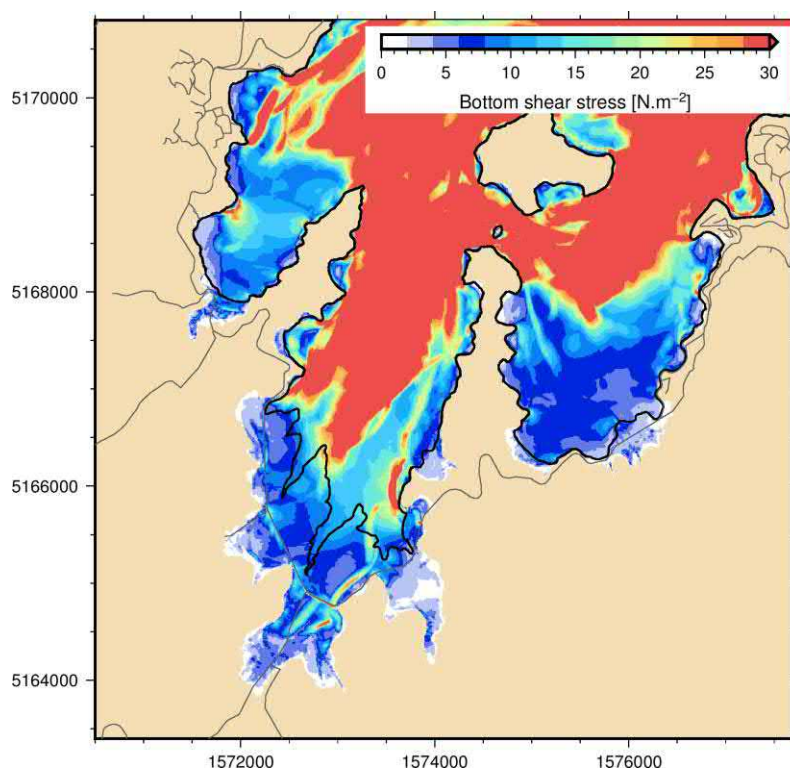


Figure 3-21: Maximum shear stress for 1:500-year return period event 2065 sea level scenario – 0.41 m sea level rise - Head of the Bay.

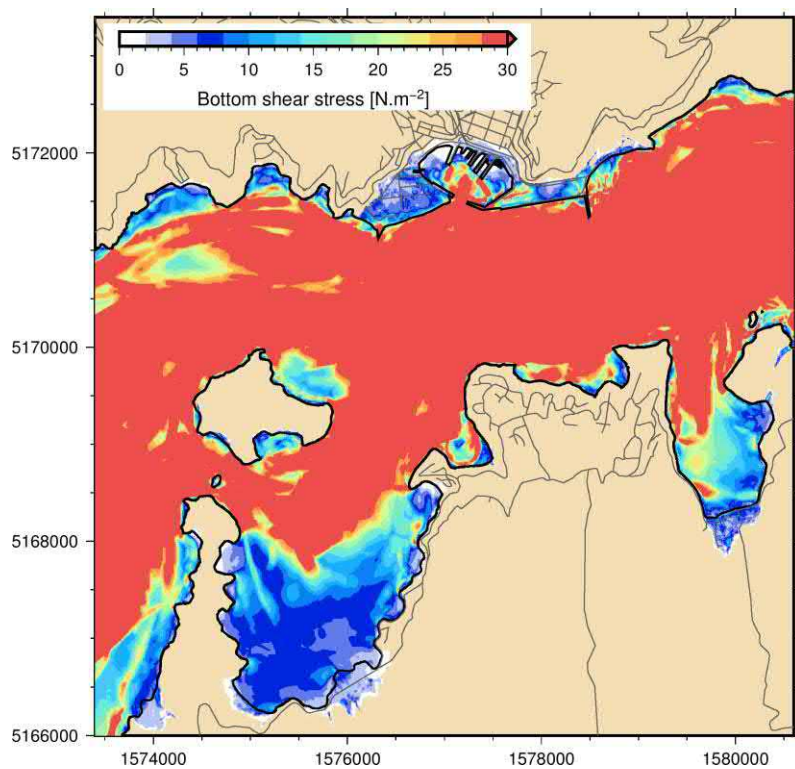


Figure 3-22: Maximum shear stress for 1:500-year return period event 2065 sea level scenario – 0.41 m sea level rise - Lyttelton and Diamond Harbour.

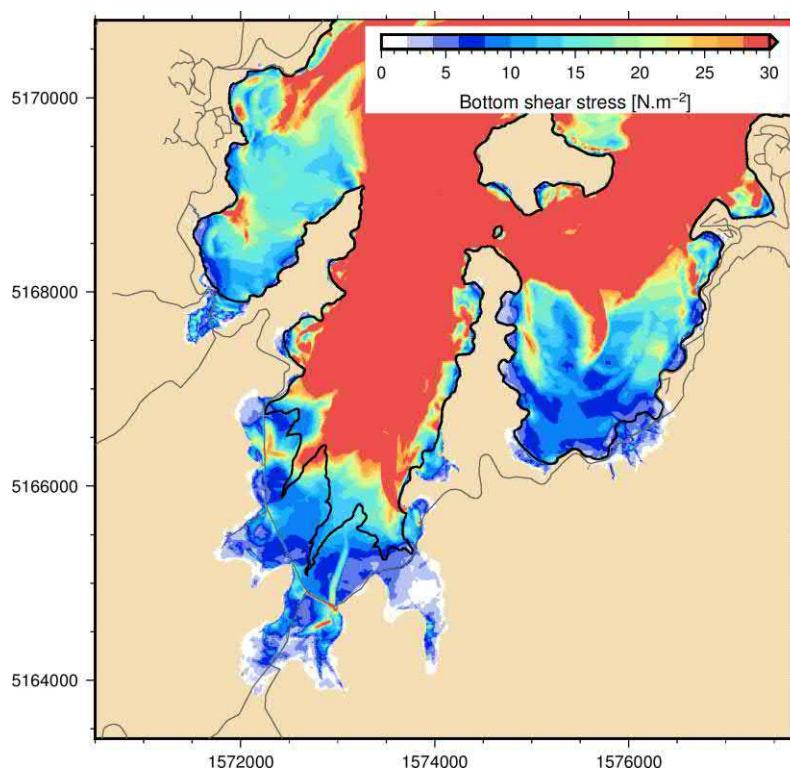


Figure 3-23: Maximum shear stress for 1:500-year return period event 2120 sea level scenario – 1.06 m sea level rise - Head of the Bay.

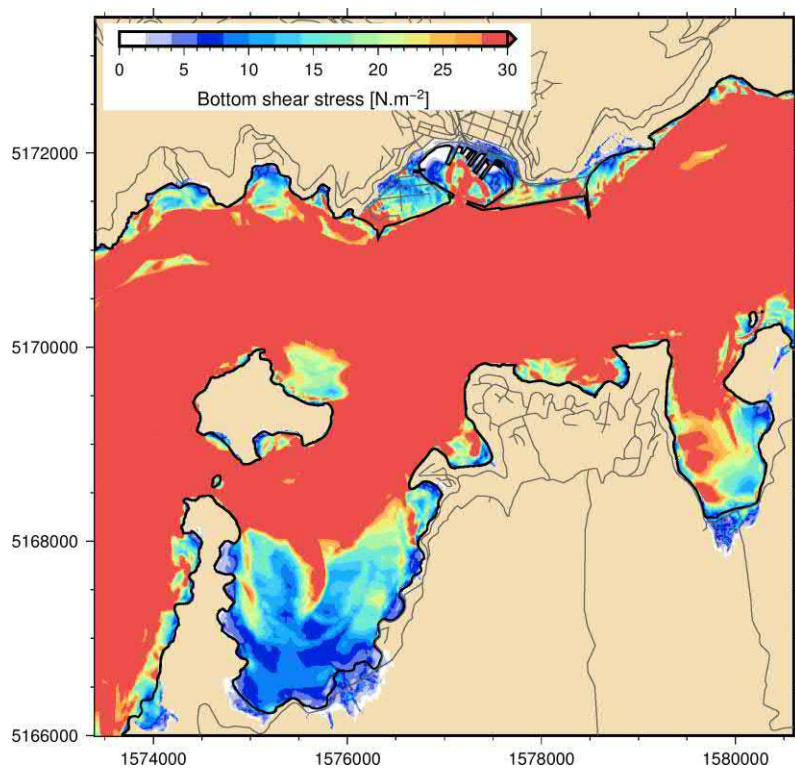


Figure 3-24: Maximum shear stress for 1:500-year return period event 2120 sea level scenario – 1.06 m sea level rise - Lyttelton and Diamond Harbour.

3.2 Akaroa Harbour

3.2.1 Inundation for 2018 sea level

Similar to Lyttelton Harbour, results indicate that low lying areas in Akaroa Harbour are the most affected by the tsunami, namely Wainui, Akaroa, Takamatua, Duvauchelle Bay, Barrys Bay and French Farm Bay. Although the tsunami scenario in this study does not produce waves in Akaroa as high as in Lyttelton (Figure 3-25, Figure 3-26), more properties are exposed to the inundation.

For the 2018 (MSL) scenario, the inundation depth in Akaroa exceeds 5.0 m and reaches as far as 250 m inland, inundating most of the historical town. North, in Takamatua, the inundation reaches beyond the Christchurch—Akaroa road as far as 440 m inland, with a maximum inundation depth of 6.5 m in the stream. In Duvauchelle, the inundation reaches 298 m inland with a maximum inundation depth of 5.7 m. In Barrys Bay the inundation extends up to 30 m inland and a maximum inundation depth of 6.0 m. In French Farm Bay, the inundation extends 300 m and reaches a maximum depth of 5.6 m. Finally, In Wainui, the inundation extent reaches 280 m with a maximum inundation depth of 3.4 m (Figure 3-27 and Figure 3-28).

3.2.2 Higher sea level scenario

As with Lyttelton Harbour, the scenarios with higher sea levels seem to amplify coastal inundation in some locations. This effect is strongest at Wainui, Akaroa, French Farm Bay and Takamatua. The effect of sea level on tsunami inundation becomes more linear in the upper harbour in Duvauchelle Bay and Barrys Bay. Inundation extent at each location reflects this effect. That is, for the 2120 sea level (MSL+1.06 m) scenario, an increase in the inundation extents of 100 m in Akaroa, 80 m in Wainui, 60 m in Takamatua, and 30 m in Duvauchelle Bay is observed. No increase is observed in Barrys Bay (Figure 3-29–Figure 3-32).

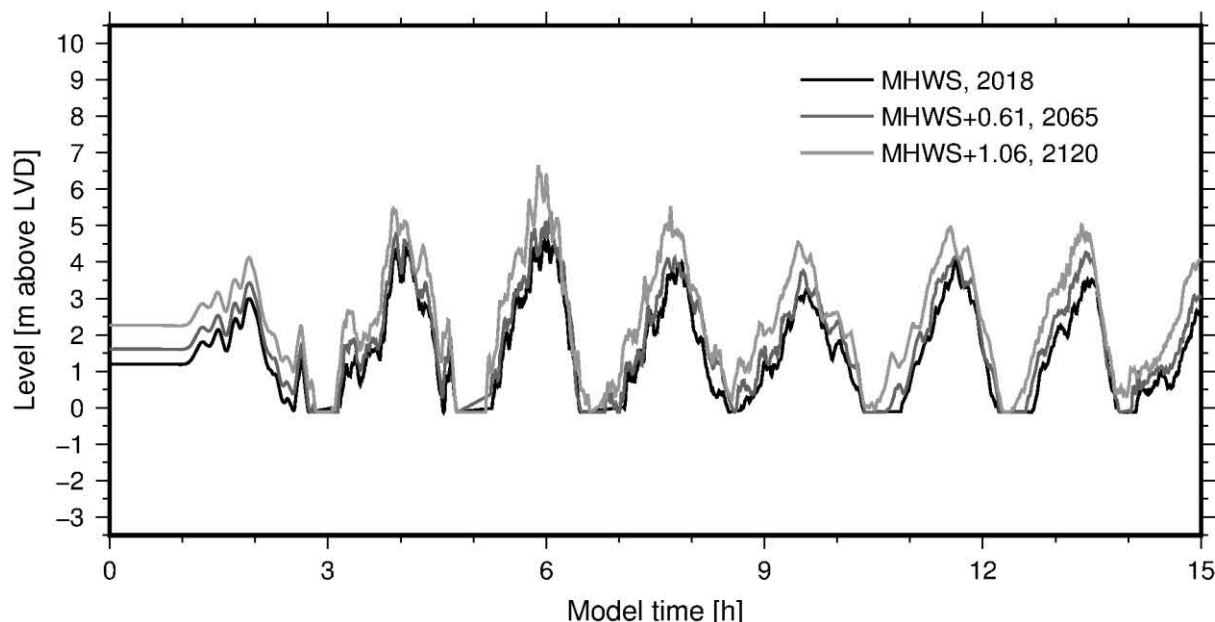


Figure 3-25: Tsunami water level at Wainui for the three sea level scenarios. The black line shows the tsunami at Mean High Water Spring (MHWS) at present mean sea level (MSL) scenario, the dark grey line shows the tsunami at MHWS for 2065 MSL (0.41 m above present MSL) scenario and the grey line shows the tsunami at MHWS for 2120 MSL (1.06 m above present MSL).

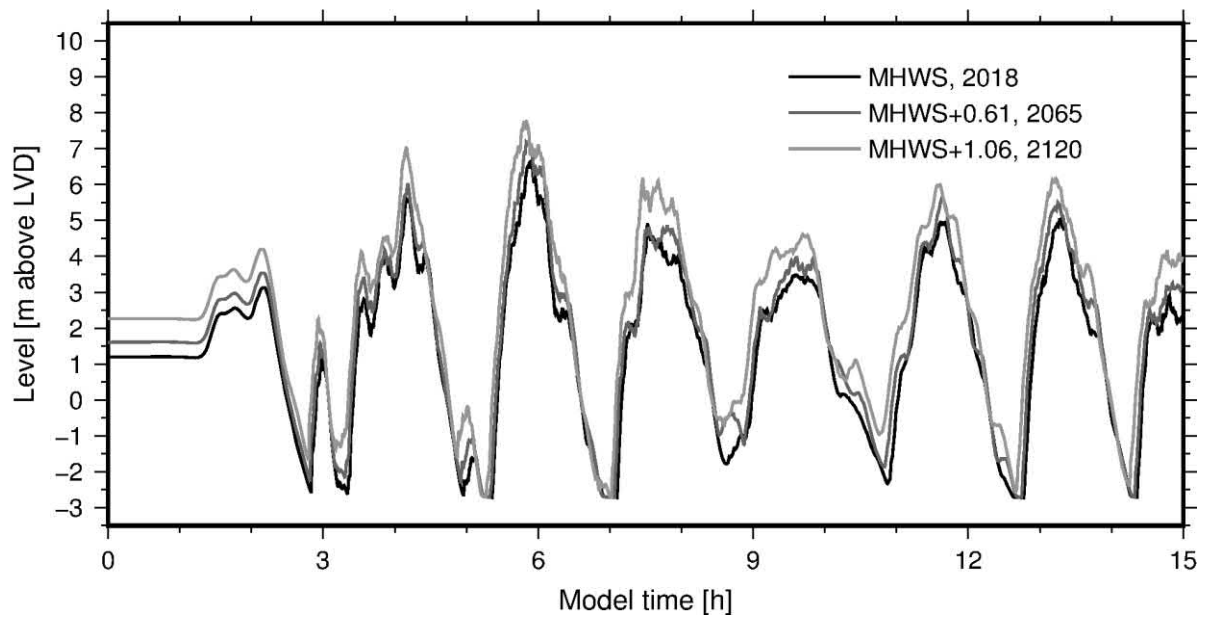


Figure 3-26: Tsunami water level at Duvauchelle Bay entrance for the three sea level scenarios. The black line shows the tsunami at Mean High Water Spring (MHWS) at present mean sea level (MSL) scenario, the dark grey line shows the tsunami at MHWS for 2065 MSL (0.41 m above present MSL) scenario and the grey line shows the tsunami at MHWS for 2120 MSL (1.06 m above present MSL).

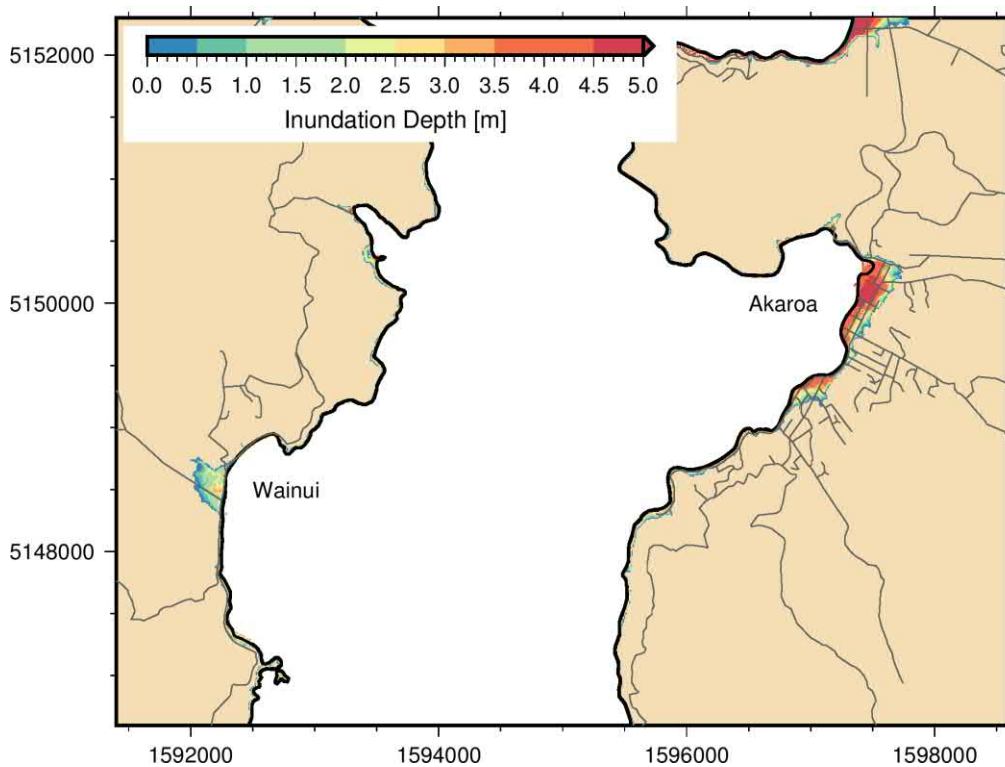


Figure 3-27: Maximum inundation depth (i.e., height above ground) for 1:500-year return period event current sea level - Wainui and Akaroa.

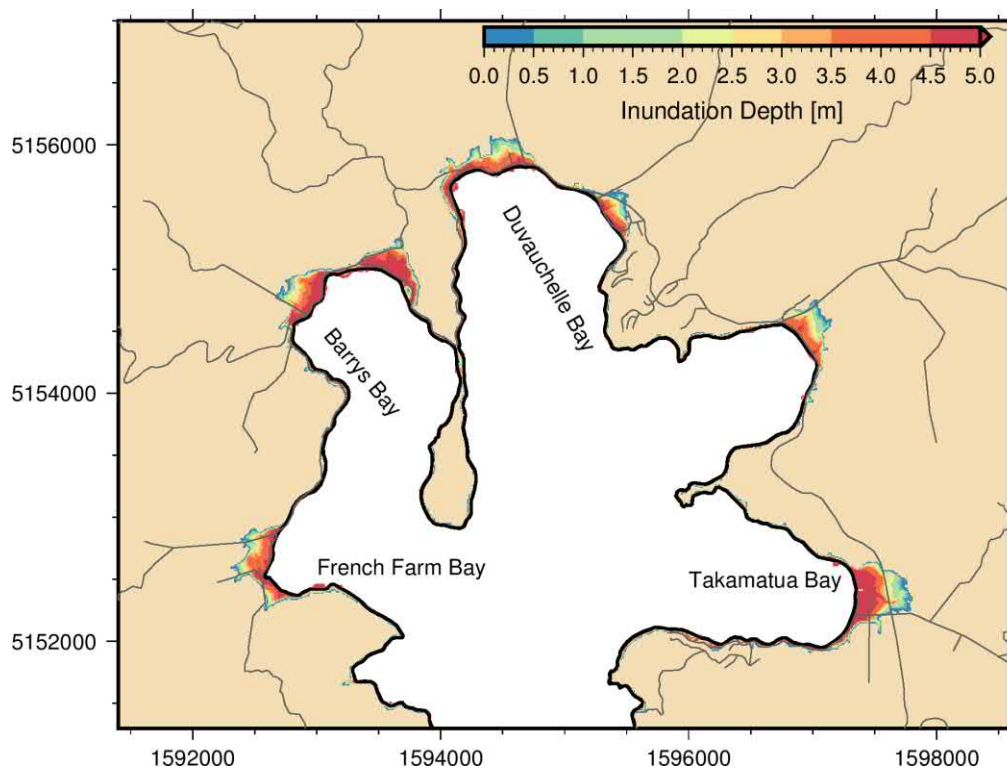


Figure 3-28: Maximum inundation depth (i.e., height above ground) for 1:500-year return period event current sea level – Upper Akaroa Harbour.

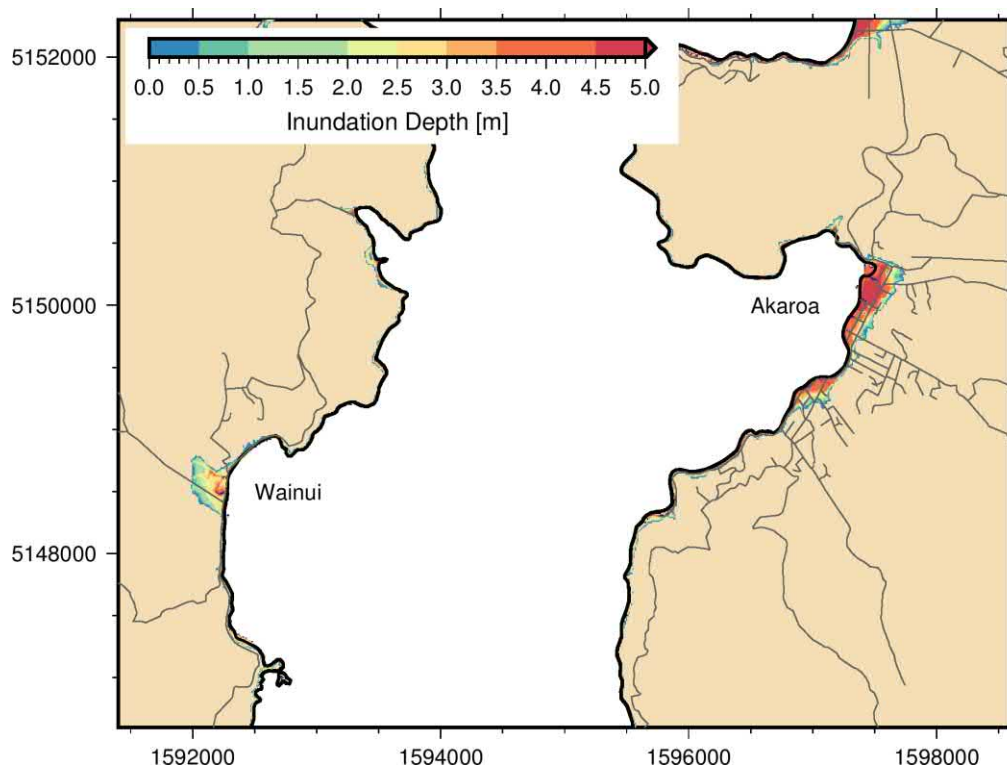


Figure 3-29: Maximum inundation depth (i.e., height above ground) for 1:500-year return period event - 2065 sea level scenario – 0.41 m sea level rise - Wainui and Akaroa. Dark blue represents current land that will

be below high tide in this sea level rise scenario. Erosional processes during the sea level rise may affect the position of the shoreline, this change is not taken into account here.

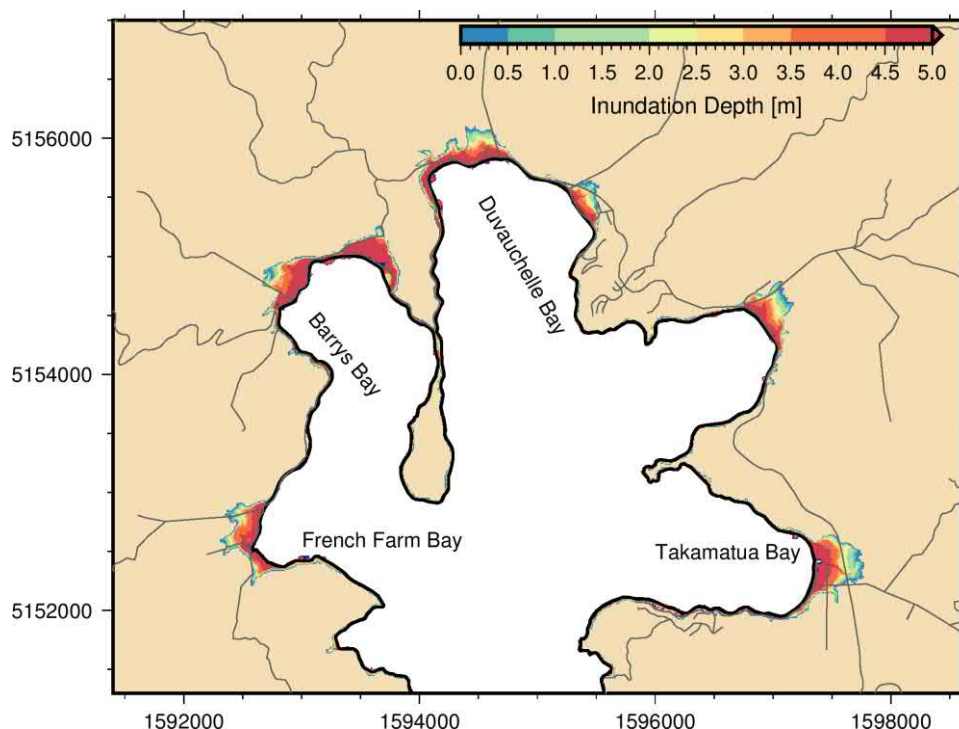


Figure 3-30: Maximum inundation depth (i.e., height above ground) for 1:500-year return period event - 2065 sea level scenario – 0.41 m sea level rise - Upper Akaroa Harbour. Dark blue represents current land that will be below high tide in this sea level rise scenario. Erosional processes during the sea level rise may affect the position of the shoreline, this change is not taken into account here.

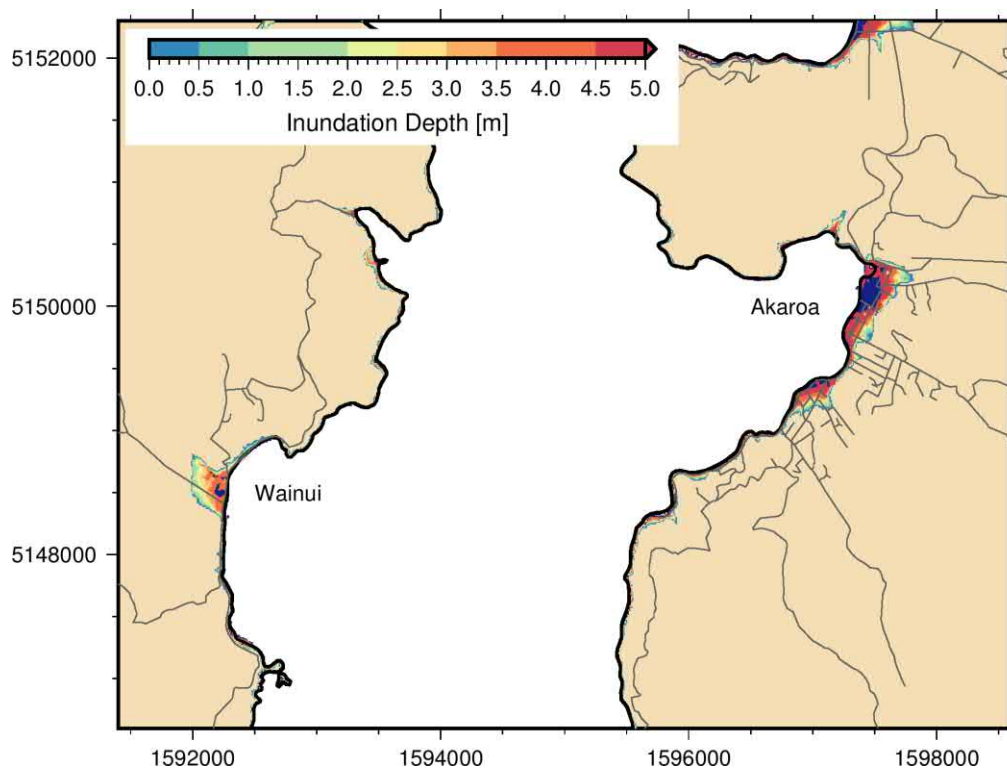


Figure 3-31: Maximum inundation depth (i.e., height above ground) for 1:500-year return period event - 2120 sea level scenario – 1.06 m sea level rise - Wainui and Akaroa. Dark blue represents current land that will be below high tide in this sea level rise scenario. Erosional processes during the sea level rise may affect the position of the shoreline, this change is not taken into account here.

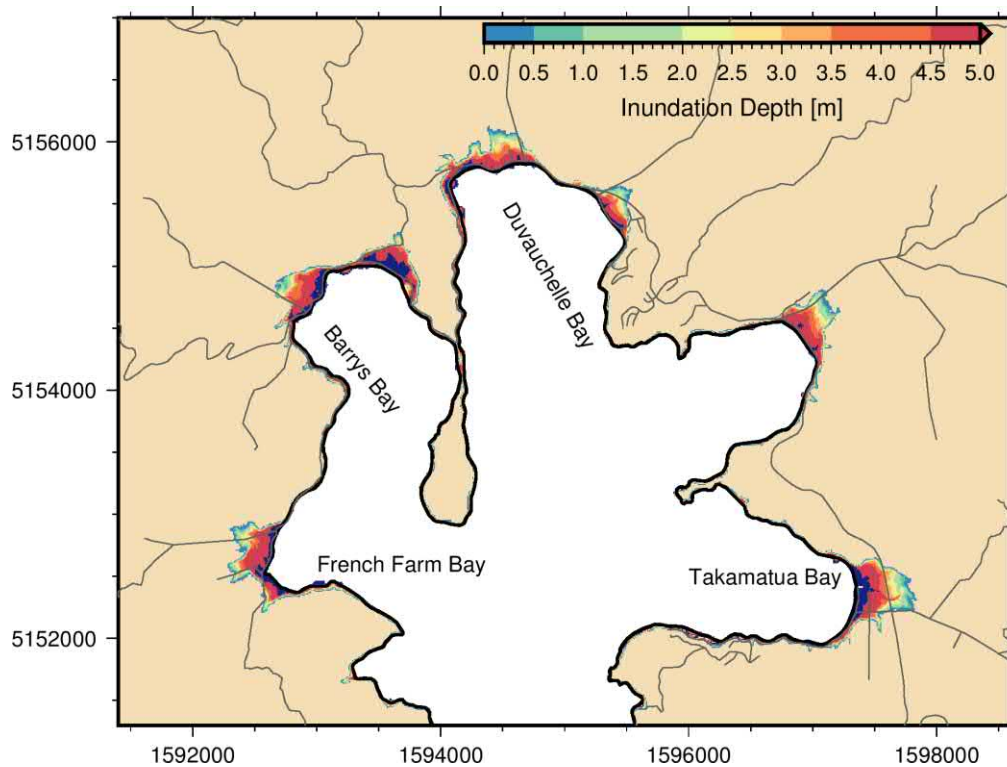


Figure 3-32: Maximum inundation depth (i.e., height above ground) for 1:500-year return period event - 2120 sea level scenario – 1.06 m sea level rise - Upper Akaroa Harbour. Dark blue represents current land that

will be below high tide in this sea level rise scenario. Erosional processes during the sea level rise may affect the position of the shoreline, this change is not taken into account here.

3.2.3 Maximum velocity

As with Lyttelton Harbour, the tsunami waves in Akaroa Harbour successively flood and drain the harbour creating very strong currents and eddies. Most of the strong velocities are located near steep bathymetry and topographic headlands.

For the present sea level scenario, results indicate that the maximum flow on the western side of the harbour between Wainui Bay and French Farm Bay exceeds 10 m/s. These high velocities are caused by eddies that form at topographic headlands and flow back and forth along the coast before dissipating. Inside the bays, the shallow water forces the flow to slow down to below 3.0 m/s (Figure 3-10, Figure 3-11).

With the higher sea level scenarios (Figure 3-37–Figure 3-40), the increased depth allows faster flows in the harbour. The location and size of the eddies are also affected. In the inundated areas, flow velocity is not greatly affected by the higher mean sea level (Figure 3-33, Figure 3-34).

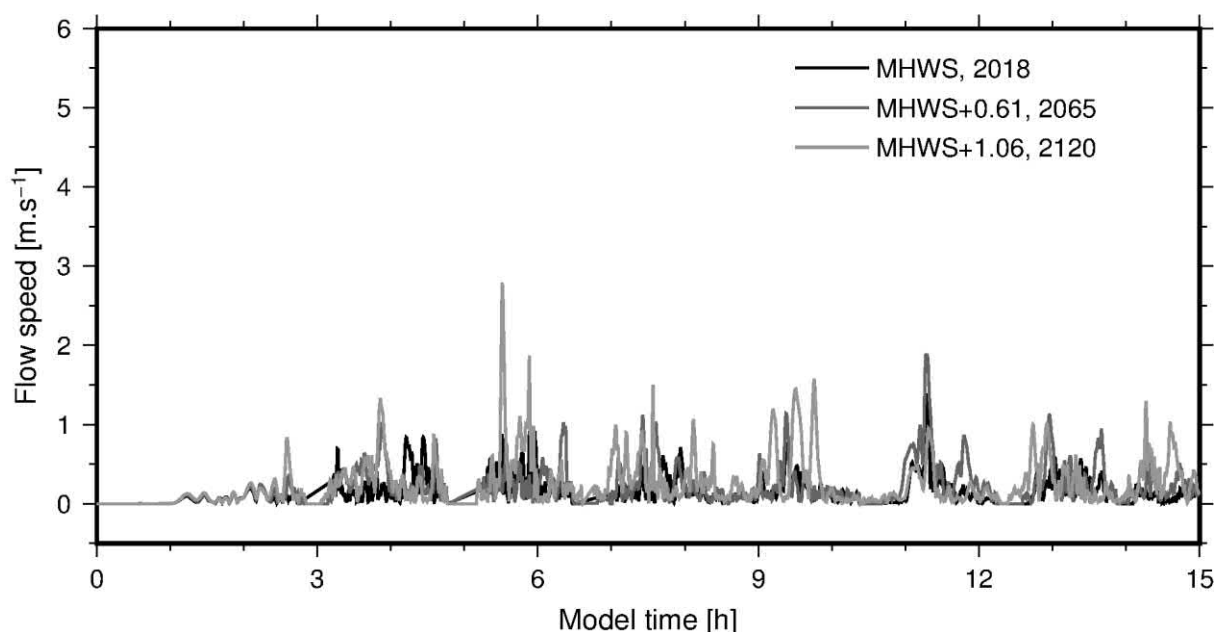


Figure 3-33: Flow velocity at Wainui for the three sea level scenarios. The black line shows the tsunami at Mean High Water Spring (MHWS) at present mean sea level (MSL) scenario, the dark grey line shows the tsunami at MHWS for 2065 MSL (0.41 m above present MSL) scenario and the grey line shows the tsunami at MHWS for 2120 MSL (1.06 m above present MSL).

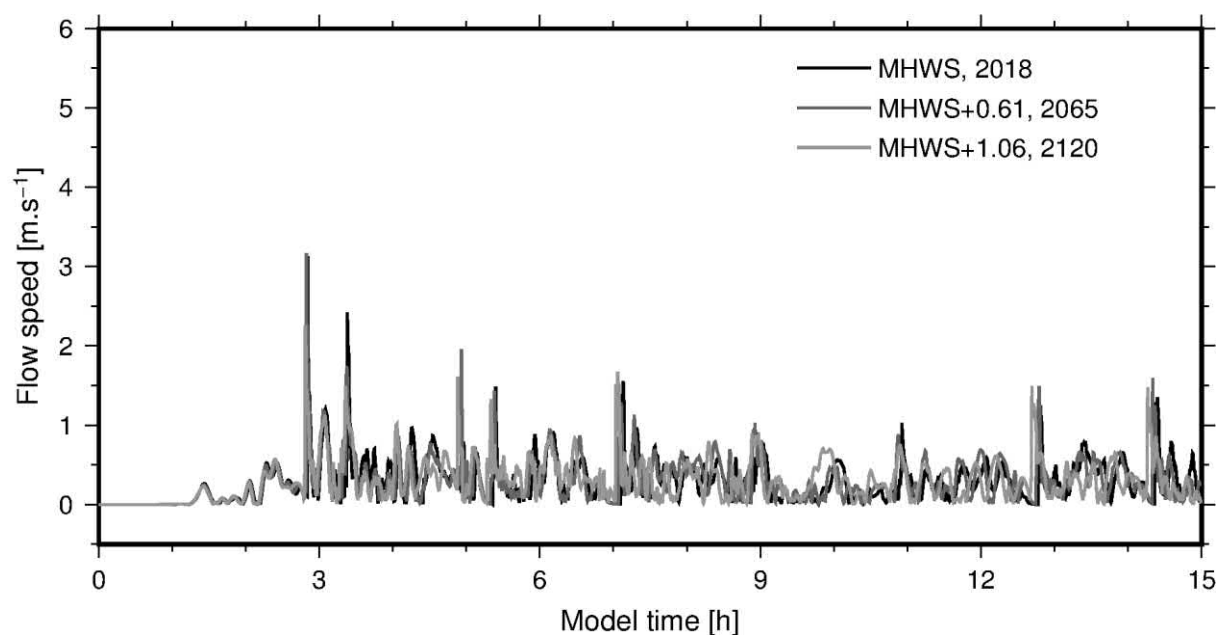


Figure 3-34: Flow velocity at Duvauchelle Bay entrance for the three sea level scenarios. The black line shows the tsunami at Mean High Water Spring (MHWS) at present mean sea level (MSL) scenario, the dark grey line shows the tsunami at MHWS for 2065 MSL (0.41 m above present MSL) scenario and the grey line shows the tsunami at MHWS for 2120 MSL (1.06 m above present MSL).

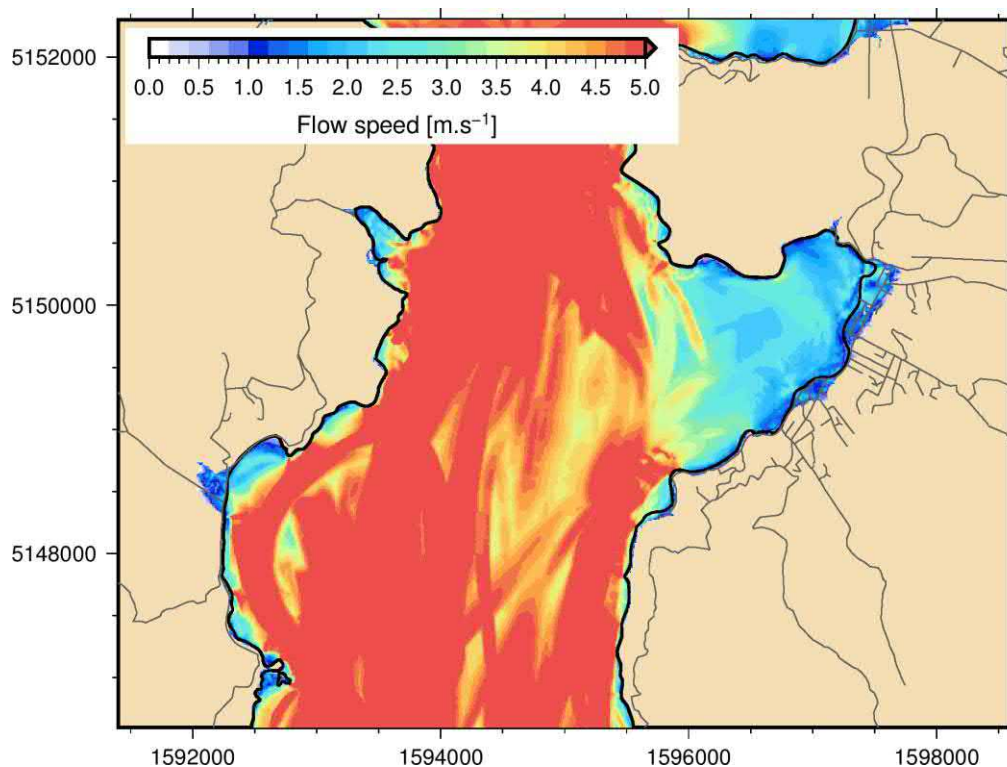


Figure 3-35: Maximum flow velocity for 1:500-year return period event current sea level - Wainui and Akaroa.

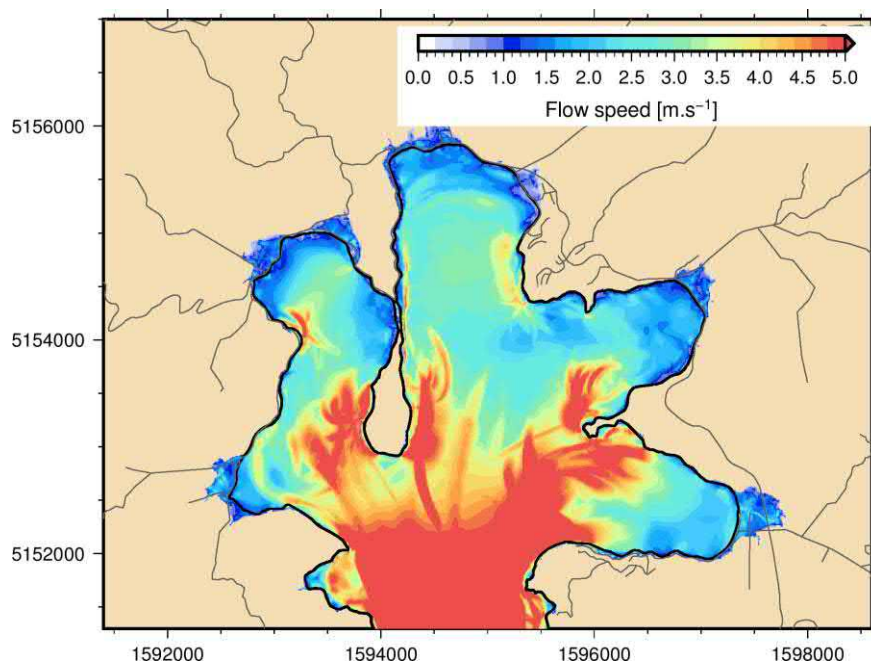


Figure 3-36: Maximum flow velocity for 1:500-year return period event current sea level - Upper Akaroa Harbour.

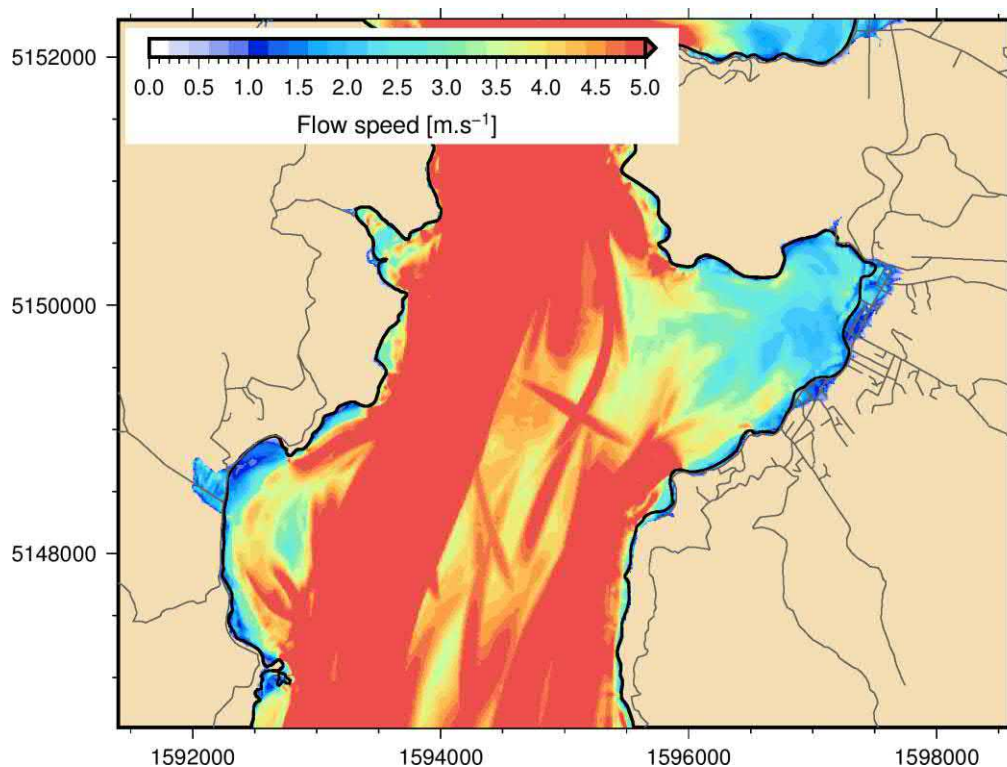


Figure 3-37: Maximum flow velocity for 1:500-year return period event 2065 sea level scenario – 0.41 m sea level rise - Wainui and Akaroa.

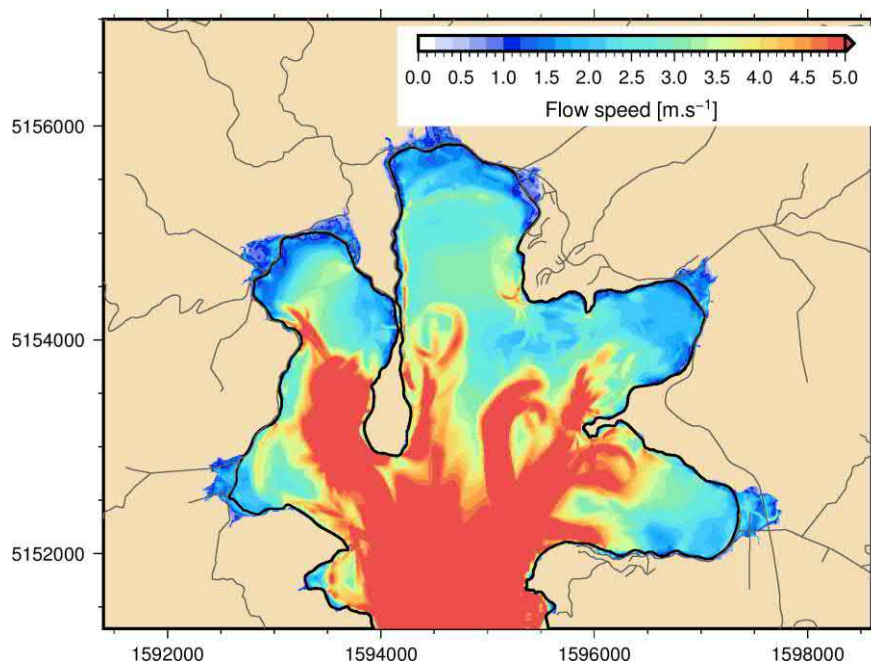


Figure 3-38: Maximum flow velocity for 1:500-year return period event 2065 sea level scenario – 0.41 m sea level rise - Upper Akaroa Harbour.

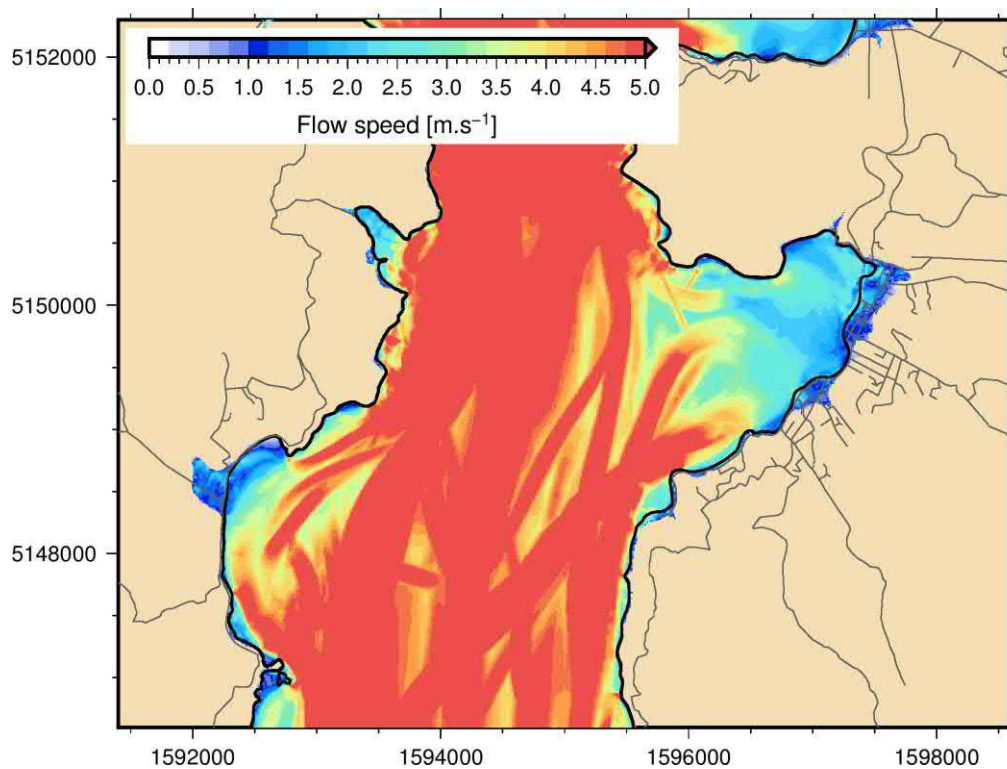


Figure 3-39: Maximum flow velocity for 1:500-year return period event 2120 sea level scenario – 1.06 m sea level rise - Wainui and Akaroa.

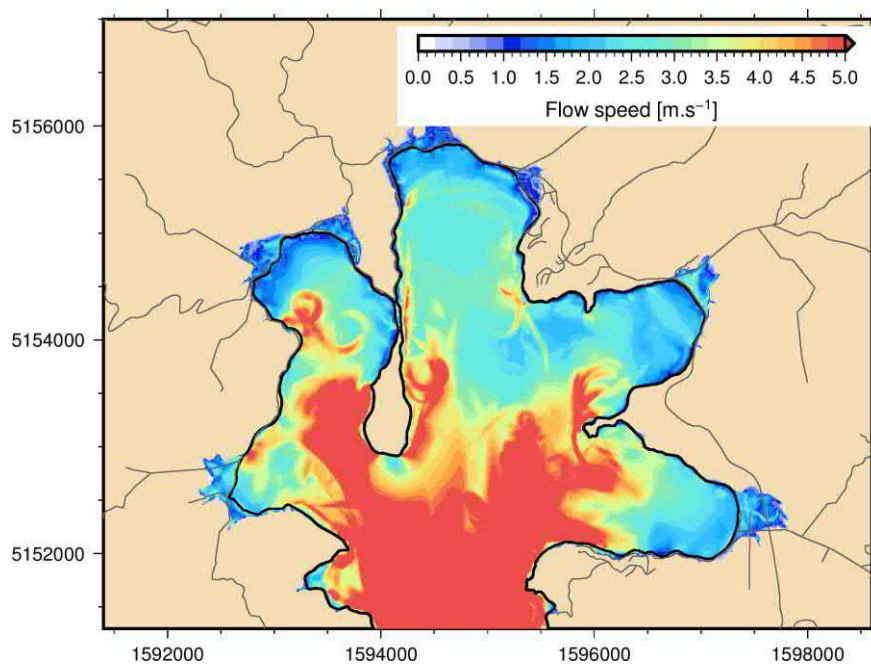


Figure 3-40: Maximum flow velocity for 1:500-year return period event 2120 sea level scenario – 1.06 m sea level rise - Upper Akaroa Harbour.

3.2.4 Erosion potential

Similar to findings in Lyttelton Harbour, the maximum shear stress for the present sea level scenario significantly exceeds the critical shear stress necessary to transport the soft sediment present in Akaroa Harbour (Figure 3-41, Figure 3-42). A large tsunami such as that simulated in this study, is expected to at least temporarily affect the morphology of the seabed throughout the harbour, especially on the neck of Bays and around headlands.

For the higher sea level scenarios (Figure 3-43–Figure 3-46), the maximum critical shear stress becomes even higher, thus amplifying the effect at present sea level.

Strong shear stresses are predicted at the shore in Duvauchelle Bay and Barrys Bay which are likely to affect the morphology of the shoreline there. In addition, return flow is likely to concentrate velocities at the mouth of streams causing large morphological changes there. In several locations, the tsunami is expected to scour parts of roads, bridges and culverts, however not enough resolution is available for a more detailed assessment.

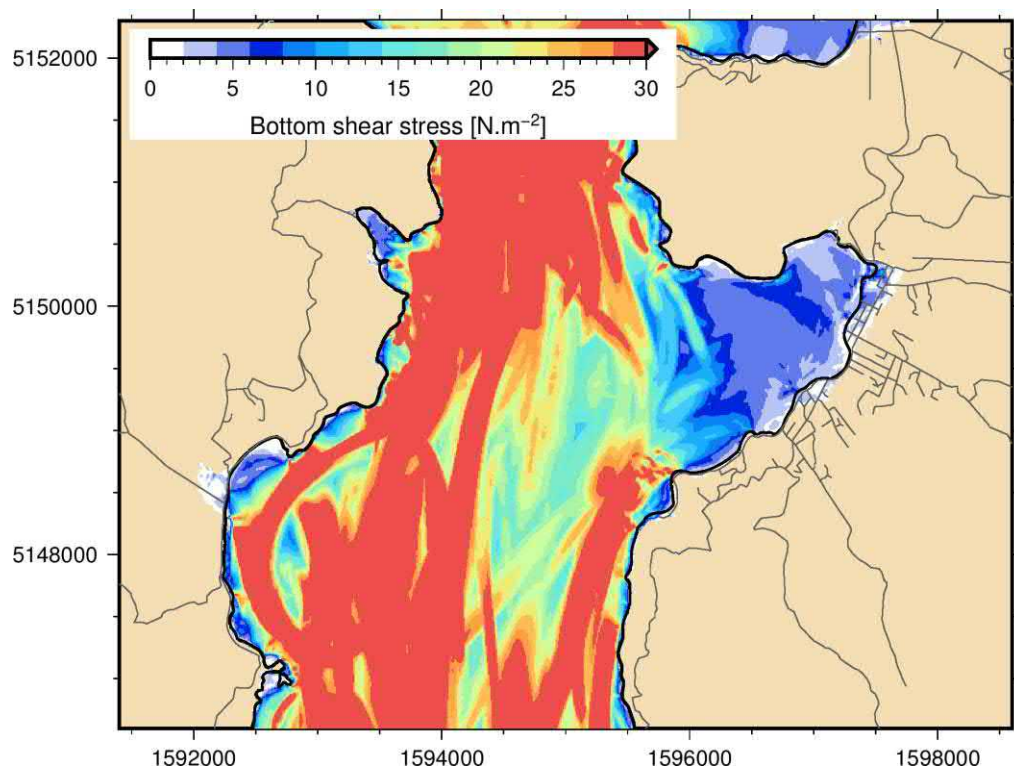


Figure 3-41: Maximum shear stress for 1:500-year return period event current sea level - Wainui and Akaroa.

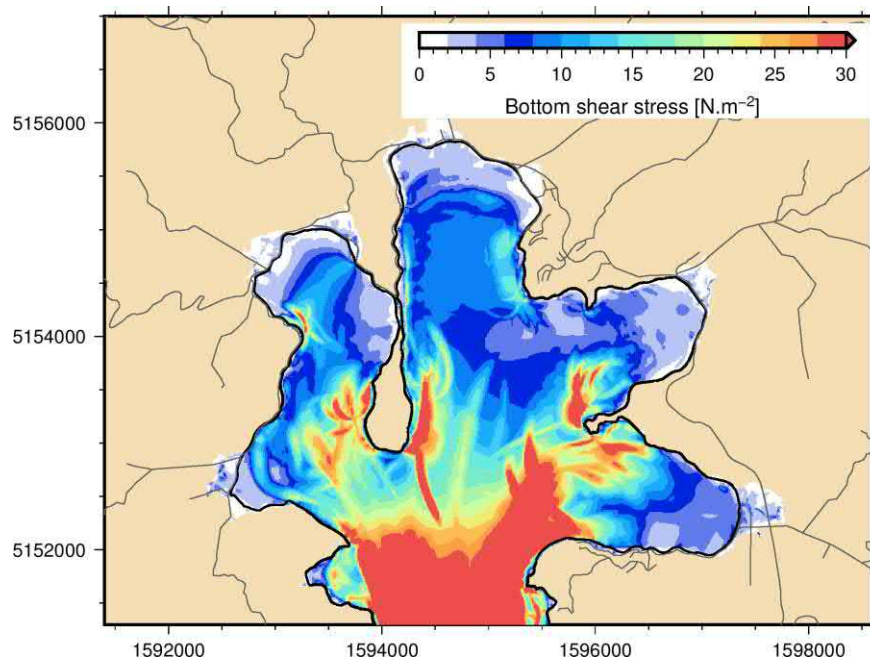


Figure 3-42: Maximum shear stress for 1:500-year return period event current sea level - Upper Akaroa Harbour.

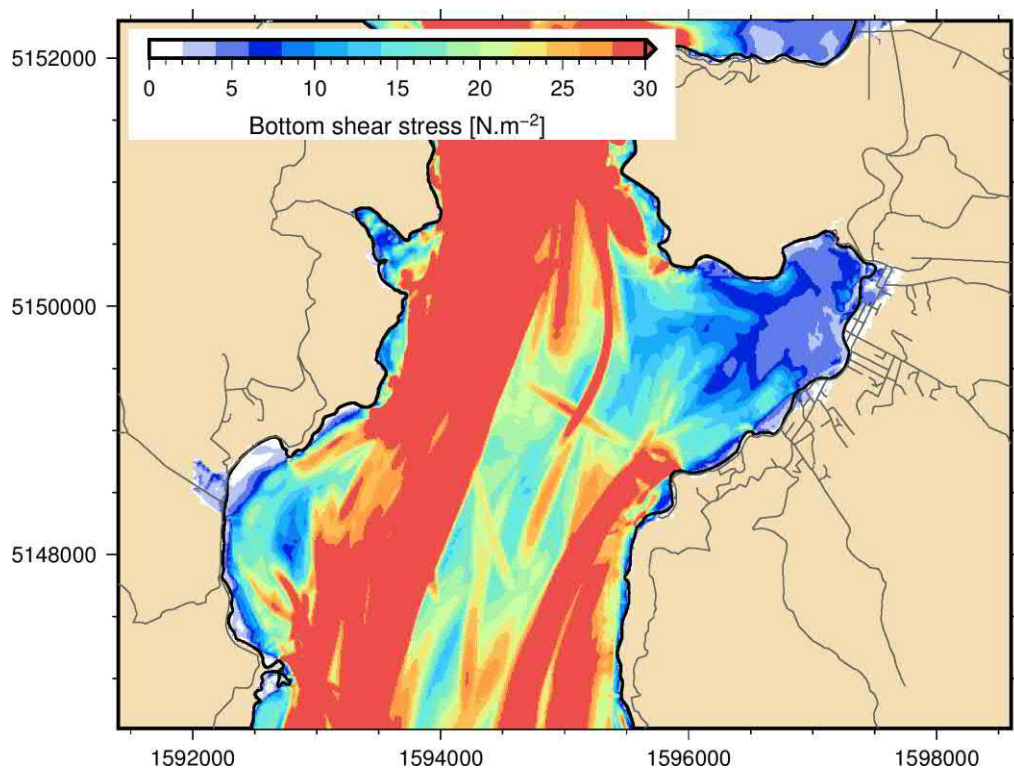


Figure 3-43: Maximum shear stress for 1:500-year return period event 2065 sea level scenario – 0.41 m sea level rise - Wainui and Akaroa.

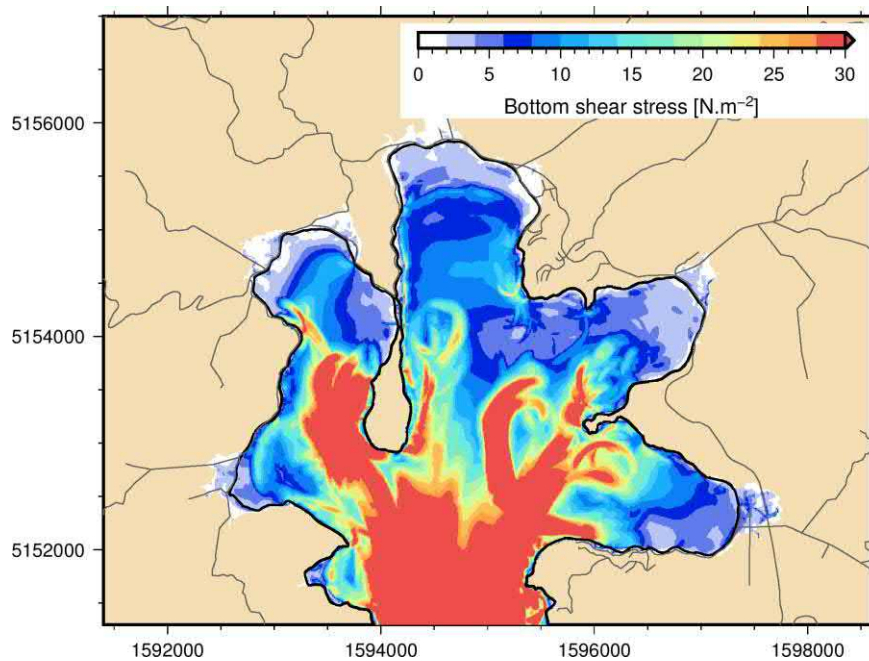


Figure 3-44: Maximum shear stress for 1:500-year return period event 2065 sea level scenario – 0.41 m sea level rise - Upper Akaroa Harbour.

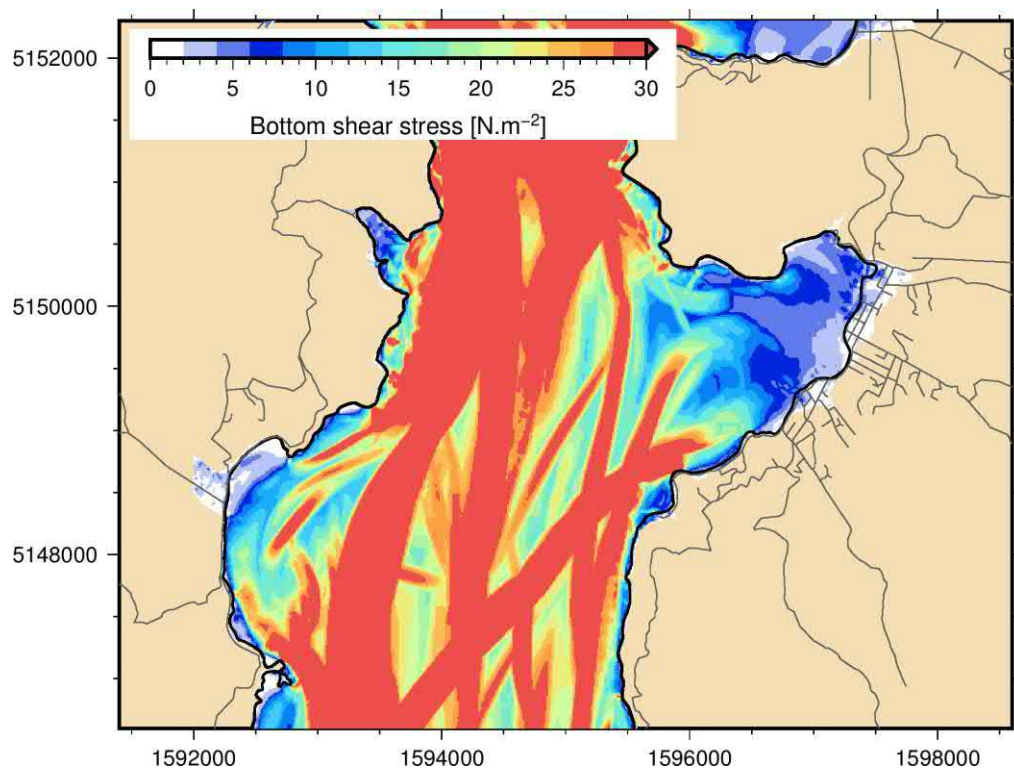


Figure 3-45: Maximum shear stress for 1:500-year return period event 2120 sea level scenario – 1.06 m sea level rise - Wainui and Akaroa.

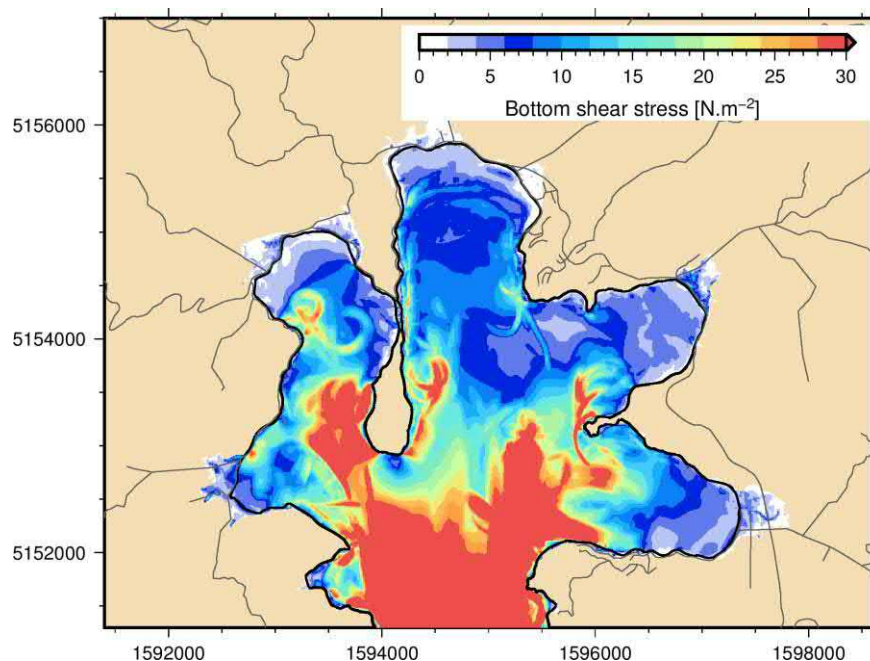


Figure 3-46: Maximum shear stress for 1:500-year return period event 2120 sea level scenario – 1.06 m sea level rise - Upper Akaroa Harbour.

4 Discussion and Conclusion

Tsunami simulation of a 1:500-year return period tsunami event originating from South America showed the inundation in Lyttelton Harbour and Akaroa Harbour for three different sea level scenarios.

In both Lyttelton and Akaroa harbours, the low-lying bays are significantly inundated by the 1:500-year event. Under sea level rise scenarios, the inundation depths are deeper even if the inundation extent does not change much due to topographic constraint.

Inundation of port areas could cause severe damage to infrastructure, especially as unattached objects like shipping containers and logs could become debris moved by the tsunami, which could impact into fixed structures exacerbating their damage and end up distributed throughout the entire harbour and beyond.

In both harbours, the tsunami wave in the upper part of the harbour was much greater than near the harbour mouth. This amplification is because, in each case, the tsunami excites the fundamental resonant mode of the harbour (Rabinovich 2008). This amplification appeared greater for the scenarios at higher sea level both in Lyttelton and Akaroa, except for the uppermost bays in Akaroa (Duvauchelle Bay and Barrys Bay) which showed an increase of the inundation depth equal to sea level rise. The amplification of the inundation with higher water level could be because the tsunami waves are better able to excite higher frequency resonant mode of the Bay. It is unclear whether this would occur with other tsunami source or how interaction with the tidal flow of the Bay (not simulated here) would affect these resonant modes.

5 References

- Bell, R.G. (2003) Planning for tsunami risk in the context of other coastal hazards. In: Cochran, U. (Ed.), Programme & Abstracts: International workshop Tsunamis in the South Pacific-Research towards preparedness and mitigation. *Institute of Geological & Nuclear Sciences Information Series* 58, p. 23. ISBN: 0478098243: 9780478098242.
- Berenbrock C., Tranmer A.W. (2008) Simulation of Flow, Sediment Transport, and Sediment Mobility of the Lower Coeur d'Alene River, Idaho. U.S. Geological Survey Scientific Investigations Report 2008–5093.
- Borrero, J.C., Goring, D.G. (2015) South American Tsunamis in Lyttelton Harbor, New Zealand. *Pure and Applied Geophysics*, 172(3–4), 757–772. <https://doi.org/10.1007/s00024-014-1026-1>.
- Bosserelle C., Arnold J., Lane E. M. (2018). Land Drainage Recovery Programme: Tsunami Study. *NIWA Client Report* No:2018039CH. Prepared for Christchurch City Council.
- De Lange W.P., Healy T.R. (1986) New Zealand tsunamis 1840–1982, *New Zealand Journal of Geology and Geophysics*, 29:1, 115–134, DOI:10.1080/00288306.1986.10427527.
- Fujii, Y., Satake, K. (2013) Slip Distribution and Seismic Moment of the 2010 and 1960 Chilean Earthquakes Inferred from Tsunami Waveforms and Coastal Geodetic Data. *Pure and Applied Geophysics*, 170(9–10), 1493–1509. <https://doi.org/10.1007/s00024-012-0524-2>.
- Gica, E., Spillane, M., Titov, V.V., Chamberlin, C., Newman, J.C. (2008) Development of the forecast propagation database for NOAA's Short-term Inundation Forecast for Tsunamis (SIFT). NOAA Tech. Memo. OAR PMEL-139, 89 pp.
- Hart D.E., Marsden I.D., Todd D.J., de Vries W.J. (2008) Mapping of the Bathymetry, Soft Sediments, and Biota of the Seabed of Upper Lyttelton Harbour. *Estuarine Research Report* 36 / ECan Report 08/35.
- Hart D.E., Todd D.J., Nation T.E., McWilliams Z.A. (2008) Upper Akaroa Harbour Seabed Bathymetry and Soft Sediments: A Baseline Mapping Study. *Coastal Research Report* 1, ECan Report 09/44, ISBN 978-1-86937-976-6.
- Lane, E.M., Kohout, A., Sykes, J., Bind, J., Williams, S.P. (2017) Distant tsunami inundation modelling incorporating dune failures and river flow in Christchurch. *NIWA Client Report* Environment Canterbury: 51.
- Lee, H.S., Shimoyama, T., Popinet, S. (2015) Impacts of tides on tsunami propagation due to potential Nankai Trough earthquakes in the Seto Inland Sea, Japan. *Journal of Geophysical Research-Oceans* 120(10): 6865–6883.
- MGD77-557371. Survey EW0001 (2000) UNOLS Rolling Deck to Repository. Project: Global and Local Controls on Depositional Cyclicity: The Canterbury Basin, New Zealand. Available at <https://www.ngdc.noaa.gov/trackline/request/?surveyIds=EW0001>.

- Popinet, S. (2011) Quadtree-adaptive tsunami modelling. *Ocean Dynamics*. Vol. 61, no. 9.: 1261-1285.
- Popinet, S. (2012) Adaptive modelling of long-distance wave propagation and fine-scale flooding during the Tohoku tsunami. *Natural Hazards and Earth System Sciences* 12(4): 1213-1227.
- Popinet, S. (2015) Basilisk. from basilisk.fr.
- Powell, D. (1998), Patterns and processes of sediment sorting in gravel-bed rivers, *Progress in Physical Geography*, 22(1), 1-32.
- Power, W. L. (2013). Review of Tsunami Hazard in New Zealand (2013 Update). GNS Science Consultancy Report 2013/131: 222.
- Power, W. L. (2014). Tsunami hazard curves and deaggregation plots for 20km coastal sections, derived from the 2013 Nation Tsunami Hazard Model. GNS Science Report
- Rabinovich, A. B. (2009) Seiches and harbor oscillations, in Handbook of Coastal and Ocean Engineering, edited by Y. C. Kim, pp. 193–236, World Sci., Singapore.
- Smith, W.H.F, Wessel, P. (1990) Gridding with continuous curvature splines in tension. *Geophysics*, 55, 293-305.
- Titov, V.V., Moore, C.W., Greenslade, D.J.M. et al. Pure Appl. Geophys. (2011) A New Tool for Inundation Modeling: Community Modeling Interface for Tsunamis (ComMIT). 168: 2121. <https://doi.org/10.1007/s00024-011-0292-4>.
- Tonkin & Taylor (2017) Coastal Hazard Assessment - Stage Two. Report for the Christchurch City Council.

6 Glossary of abbreviations and terms

Flow depth	Vertical height of tsunami above land (also known as inundation depth)
Inundation depth	Vertical height of tsunami above land (also known as flow depth)
Inundation extent	Horizontal distance from shoreline to maximum inland extent of tsunami
Run-up height	Vertical height the tsunami reaches above mean sea level at the limit of inundation. Runup is dependent on the type of wave and local bathymetry
Tsunami water level	Vertical height of the tsunami above mean sea level

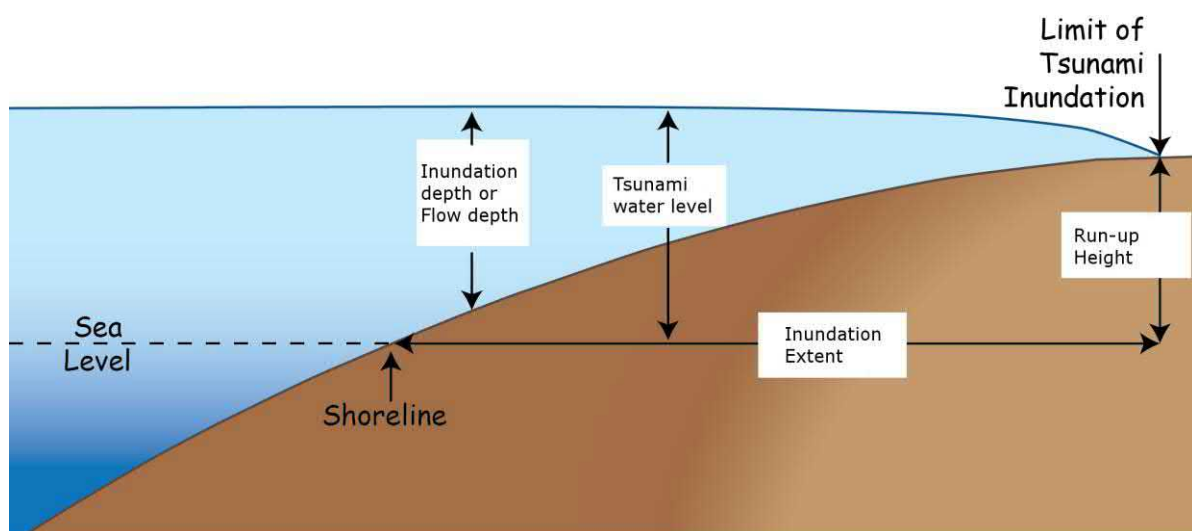


Figure 6-1: Tsunami inundation terminology.